Single-cone finite-difference schemes for the (2+1)-dimensional Dirac equation in general electromagnetic textures

Walter Pötz
Institut für Physik, Karl-Franzens-Universität Graz, Universitätsplatz 5, 8010 Graz, Austria
(Received 8 August 2017; published 27 November 2017)

A single-cone finite-difference lattice scheme is developed for the (2+1)-dimensional Dirac equation in presence of general electromagnetic textures. The latter is represented on a (2+1)-dimensional staggered grid using a second-order-accurate finite difference scheme. A Peierls-Schwinger substitution to the wave function is used to introduce the electromagnetic (vector) potential into the Dirac equation. Thereby, the single-cone energy dispersion and gauge invariance are carried over from the continuum to the lattice formulation. Conservation laws and stability properties of the formal scheme are identified by comparison with the scheme for zero vector potential. The placement of magnetization terms is inferred from consistency with the one for the vector potential. Based on this formal scheme, several numerical schemes are proposed and tested. Elementary examples for single-fermion transport in the presence of in-plane magnetization are given, using material parameters typical for topological insulator surfaces.

DOI: 10.1103/PhysRevE.96.053312

I. INTRODUCTION

Recently a staggered space-time grid has been identified which enables the formulation of single-cone finite-difference schemes for the $(d+1)$-dimensional Dirac equation [1]. Here $(d+1)$-dimensional refers to d space and one time dimension. Explicit second-order-accurate schemes have been presented and characterized for $d = 1,2,3$ in the presence of mass- and scalar potential terms [1,2]. This is remarkable because traditional real-space lattice schemes used for Dirac fermions, for example, in quantum chromo-dynamics simulations on a lattice, in general display fermion doubling [3]. To our knowledge, in standard simulations based on finite difference schemes, the unphysical doublers hitherto have been projected out by a method suggested by Susskind and Kogut, were pushed out of the energy range of interest by a mass term, the chiral symmetry-breaking Wilson term, or have been avoided at the expense of nonlocality [4–7].[1] As an alternative to finite-difference methods, other numerical approaches for solving the time-dependent Dirac equation, such as the operator-splitting and Lanczos method, have been developed [8–10]. Within the former, fermion doubling can be avoided by fast Fourier transformation between momentum and position representation in the evaluation of the time evolution operator. To our knowledge, scaling is $N \log N$, as compared to linear in the number of grid points N, for the staggered finite-difference scheme. The Lanczos method apparently can approach this efficiency, however, in a real-space representation avoidance of fermion doubling remains to be an issue.

Recent Dirac fermion realizations in condensed matter systems, such as graphene and topological insulators (TIs), have generated great interest in transport simulations based on the (2+1)-dimensional Dirac equation [11–14]. In this context, the Dirac equation describes (metallic) low-energy excitations which have several remarkable properties. A magnetic field perpendicular to the surface can be used to introduce a space-time-dependent mass term. It has been used to engineer and manipulate the surface states, as well as the associated Dirac fermion dynamics [15–22]. The odd number of cones and momentum-spin locking associated with TI surface states point at inherent potential for spintronics applications.

The development of single-cone lattice models is of fundamental importance in physics. Additional motivation for this work has been provided by the realization of Dirac fermion states on TI surfaces. With the construction of single-cone lattice models established in earlier work, in this article we address several issues: the development of a finite-difference scheme for the time-dependent (2+1)-dimensional Dirac equation in the presence of general electromagnetic texture, in particular, the presence of magnetic fields and magnetization which (1) preserves the single-cone energy-momentum dispersion and (2) is gauge-invariant, as well as (3) the analysis of the stability properties of such a scheme. It will be shown that, in analogy to the continuum case, a Peierls-Schwinger substitution can be used to formally introduce both vector potential and magnetization. Since this substitution is a $U(1)$ transformation, all stability properties of the free-particle scheme are preserved. This formal scheme is the basis for several physically motivated approximations on the lattice. They facilitate space-time-resolved simulations of spintronic effects associated with TI Dirac fermions near the Dirac point.

In Sec. II we give a brief review of the (2+1)-dimensional Dirac equation in the TI representation. In Sec. II B we summarize the necessary ingredients for a single-cone finite-difference scheme. In Sec. III we present the formal scheme containing the full electromagnetic potential, identify a conserved functional, and discuss stability properties and gauge invariance of the scheme. Its explicit form including lattice indices is given in the Appendix. Based on the formal scheme several lattice schemes are derived in Sec. IV: (1) a scheme for static planar magnetic texture, (2) a single-time-update scheme, (3) a double-time-update scheme, and (4) a "slowly varying-magnetic-field scheme" valid under slowly varying

[1]Here "unphysical" implies that these (counterpropagating) modes are absent in the underlying continuum model.

planar texture. In Sec. V we numerically test and compare these schemes for a rotating uniform planar magnetization which allows solution within the formal scheme. Finally, we consider a static planar magnetic texture and compare the static model (1) to the slowly varying-magnetic-field model (4).

II. THEORETICAL BACKGROUND

A. The model Hamiltonian and its physical properties

The low-energy dynamics of Dirac fermions on a magnetically textured surface of a topological insulator is captured by an effective (2+1)-dimensional Dirac equation [13]. A magnetization, which may arise from magnetic impurities near the surface, is treated within a mean-field approximation. The effective fermion Hamilton operator consists of a spin-orbit, a Zeeman-Pauli, and a scalar potential term and has the form [23]

$$H = c(\boldsymbol{\sigma} \times \boldsymbol{\Pi}) \cdot \hat{\mathbf{z}} + \mu_B g_F \boldsymbol{\sigma} \mathbf{B}'(x,y,t) + V(x,y,t). \quad (1)$$

Here c, $\boldsymbol{\sigma}$, μ_B, g_F, and $V \in \mathbb{R}$, respectively, are the fermion speed, the Pauli vector, the Bohr magneton, the fermion Landé factor, and the potential energy. $\hat{\mathbf{z}}$ denotes the unit vector normal to the TI surface which is assumed to be a plane. In the spin-orbit term,

$$\boldsymbol{\Pi} = \mathbf{p} - \frac{q}{c_o}\mathcal{A} \quad (2)$$

denotes the fermion kinetic momentum operator. Here we have charge $q = -e$ for the Dirac electron. $\mathbf{p}$, c_o, e, and $\mathcal{A}$, respectively, denote the canonical momentum operator, the speed of light in vacuum, the elementary charge, and the vector potential. The magnetic field $\mathbf{B}(x,y,t) = \boldsymbol{\nabla} \times \mathcal{A}(x,y,z,t)|_{z=0} = \mathbf{B_o}(x,y,t) + 4\pi\mathcal{M}(x,y,t)$ results from the external B-field B_o and the stray field from the impurities' magnetization $\mathcal{M}(x,y,t)$.

The effective magnetic field in the Pauli term is given by

$$\mathbf{B}'(x,y,t) = \mathbf{B_o}(x,y,t) - \frac{1}{g_F \mu_B} \sum_i \langle J_i' \mathbf{S}_i \rangle \boldsymbol{\sigma}, \quad (3)$$

in which the second contribution is the effective exchange field between fermion spin and the impurity spin $\mathbf{S}_i$ with exchange coupling J_i'. In the presence of ferromagnetic order, the dominant coupling to the effective magnetic field is due to the Pauli term [23].

In Schrödinger form a generic version of the effective Dirac equation reads

$$i\hbar\partial_t \boldsymbol{\psi}(x,y,t) = [c(\sigma_x \Pi_y - \sigma_y \Pi_x) + \boldsymbol{\sigma} \cdot \mathbf{m}(x,y,t) + \mathbb{1}_2 V(x,y,t)]\boldsymbol{\psi}(x,y,t). \quad (4)$$

$\boldsymbol{\psi}(x,y,t) \equiv [u,v] \in \mathbb{C}^2$ is a two-component spinor describing the helical states associated with a single Dirac cone. The two components correspond to spin $= 1/2$, whereby the physical spin direction is $\mathbf{S} \propto \boldsymbol{\sigma}$ and, from Eq. (1), $\mathbf{m}(x,y,t) = \mu_B g_F \mathbf{B}'(x,y,t)$. Note that an in-plane magnetization coupling to the fermion spin formally can be incorporated into the vector potential term in the kinetic momentum and vice versa. However, the sources for these two terms may have a different physical origin and consequences.

In the TI basis the current density vector has the components

$$j_x = -c(u^*, v^*)\sigma_y \begin{pmatrix} u \\ v \end{pmatrix} = -2c\,\mathrm{Im}\{u^* v\},$$
$$j_y = c(u^*, v^*)\sigma_x \begin{pmatrix} u \\ v \end{pmatrix} = 2c\,\mathrm{Re}\{u^* v\}. \quad (5)$$

Note that they do not contain an explicit contribution from the magnetization or vector potential, but rather result from the phase relation between the two spinor components. Likewise, the expectation value for the particle spin, orthogonal to the current density, is given by

$$S_x = \frac{\hbar}{2}(u^*, v^*)\sigma_x \begin{pmatrix} u \\ v \end{pmatrix} = \hbar\,\mathrm{Re}\{u^* v\},$$
$$S_y = (u^*, v^*)\sigma_y \begin{pmatrix} u \\ v \end{pmatrix} = \hbar\,\mathrm{Im}\{u^* v\}. \quad (6)$$

One sees that spin and momentum are "locked to one another" at a right angle. Therefore, changing the direction of particle flow changes the direction of spin-polarization and vice versa.

B. Staggered grid for a single-cone finite-difference scheme

Here we give a brief review of the single-cone lattice representation of the (2+1)-dimensional Dirac equation underlying the present work. It is well known that a symmetric discretization of first-order derivatives using twice the lattice constant leads to an increase in the degrees of freedom as compared to the continuum formulation. In the case of the Dirac equation one speaks of fermion doubling [5,6]. Early attempts to work around this problem have been the use of an artificial mass term or projection techniques [4,5]. The Wilson mass term is a finite difference approximation to a second-order derivative which uses the single lattice constant, thereby lifting the degeneracy between physical modes and doublers. In the Susskind and Kogut method of staggered fermions, the effective lattice constant is doubled leading to 2^{d+1} lattice sites within a hypercube. Subsequently the extra lattice sites are used to introduce additional flavors of fermions [24]. For example, in $d = 3$ one has four spinor components per fermion and 2^4 lattice sites per space-time hypercube, leading to four flavors of fermions on the lattice. One can then either use the extra lattice sites to incorporate different physical flavors, e.g., quarks, or consider the extra degrees of freedom as unphysical and project them out.[2]

In contrast to the Susskind and Kogut staggered fermions, in the present approach, the original lattice constants are maintained and used to approximate all first-order derivatives. In essence, the original rectangular grid is converted into a set of a face-centered rectangular-grid double-layers (Fig. 1) [1]. This single-cone finite-difference scheme is a leap-frog scheme based on a space-time staggered grid which allows all first-order partial derivatives to be represented by symmetric difference quotients using a single lattice spacing, making it second-order accurate. Originally, it was developed for the

[2]We note that there is a lattice scheme in the literature which falsely claims to be single cone [25].

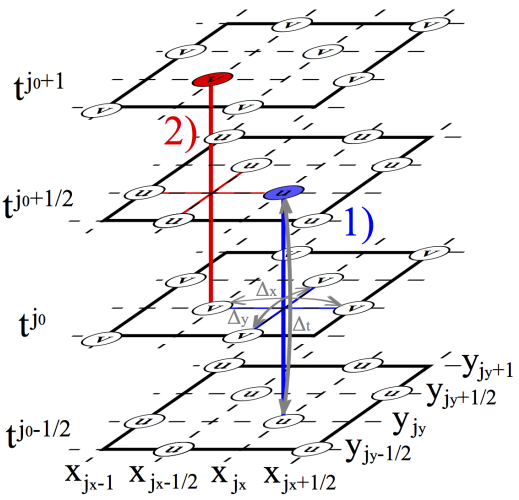

FIG. 1. Sketch of the staggered grid needed to propagate a two-component spinor $\boldsymbol{\psi} \equiv [u,v]$ by one time step Δ_t. Placing upper and lower components onto the adjacent time sheets, respectively, $t^{j_o-\frac{1}{2}}$ and t^{j_o} allows the propagation to the next pair of time sheets via spatial derivatives, represented by single lattice spacings (Δ_x and Δ_y), in two steps: the upper spinor component u from subgrid $j_o - \frac{1}{2}$ to $j_o + \frac{1}{2}$, followed by the lower spinor component v from subgrid j_o to $j_o + 1$.

case of zero vector potential [1]. For the (2+1)-dimensional case one may proceed as follows (for details we refer to the original paper): the spinor u-component is defined for the discrete time indices $j_o - \frac{1}{2} \in \mathbb{Z} + \frac{1}{2}$ and lives on the discrete lattice points $(j_x, j_y) \in \mathbb{Z}^2$ and $(j_x - \frac{1}{2}, j_y - \frac{1}{2}) \in (\mathbb{Z} + \frac{1}{2})^2$, forming a face-centered rectangular (fcr-u) grid for each time sheet. The spinor v-component is defined for discrete time $j_o \in \mathbb{Z}$ and space indices $(j_x - \frac{1}{2}, j_y) \in (\mathbb{Z} + \frac{1}{2}) \times \mathbb{Z}$ and $(j_x, j_y - \frac{1}{2}) \in \mathbb{Z} \times (\mathbb{Z} + \frac{1}{2})$, again forming a face-centered rectangular (fcr-v) grid. As sketched in Fig. 1 the time progression by $\Delta_o = c\Delta_t$ is executed in two steps: First, the upper component u is propagated from time sheet $j_o - \frac{1}{2}$ to $j_o + \frac{1}{2}$ (each consisting of a fcr-u grid) by forming symmetric x- and y-derivatives of v using the fcr-v grid on intermediate time sheet j_o. In the second step, v on the fcr-v grid on time sheet j_o is propagated to the fcr-v grid on time sheet $j_o + 1$ using symmetric x- and y-derivatives of u on the fcr-u grid on time sheet $j_o + \frac{1}{2}$. Altogether, one has to propagate $u^{j_o-\frac{1}{2}}_{j_x,j_y}$, $u^{j_o-\frac{1}{2}}_{j_x+\frac{1}{2},j_y+\frac{1}{2}}$, $v^{j_o}_{j_x+\frac{1}{2},j_y}$, and $v^{j_o}_{j_x,j_y+\frac{1}{2}}$ for $j_v \in \mathbb{Z}$. Here, and in the generalization below, we use the following notation for any quantity placed on the grid: the superscript contains the time index, and the index pair in the subscript gives the lattice site (spatial position) on the specified time sheet. For further details, we refer to earlier work [1].

Note that on the grid a specific u-component, say, $u^{j_o+1/2}_{j_x,j_y}$, is not linked to a unique v component: there are four nearest neighbor v-sites on each of the two adjacent v-time sheets j_o and $j_o + 1$. This symmetry is taken into account when computing local single-particle averages, such as particle, current, and spin density. Note that this nonlocality in the lattice (field-) theory is required to bypass the Nielssen-Ninomiya theorem [26]. Furthermore, our scheme treats space and time derivatives on equal footing, as suggested by covariance of the Dirac equation, leading to the use of two time sheets to store the spinor "at given time," as shown in Fig. 1. Yet the propagation scheme is explicit and allows local, grid-point-by-grid-point, layer-by-layer execution.

The importance of a genuine single-cone scheme is not merely founded on physical consistency with the continuum model but also on technical aspects. Spurious modes ("doublers") can have counterpropagating group velocities, a fact which complicates the construction of transparent or absorbing boundary conditions in open-boundary transport simulations. For the (1+1)-dimensional and (2+1)-dimensional case, respectively, transparent and perfectly matched-layer boundary conditions have already been constructed within this single-cone scheme [2,27,28].

III. FORMAL SCHEME FOR THE (2+1)-DIMENSIONAL DIRAC EQUATION

A. Definition

In this section we develop a finite-difference scheme for (2+1)-dimensional Dirac fermions in general electromagnetic texture. The (2+1)-dimensional scheme or Ref. [1] serves for a skeleton which is dressed by a Peierls-Schwinger substitution [24]. The procedure may be summarized as follows: Apply a Schwinger-Peierls substitution to the Dirac spinor, and insert the transformed spinor into the single-cone staggered-grid lattice scheme of Ref. [1] for the free-particle Hamiltonian. Express the scheme in terms of the original spinor components eliminating the path-dependent Peierls-Schwinger phase factor.

The gauge-invariant introduction of the electromagnetic potential into the free-particle Hamiltonian is accomplished by the Schwinger substitution [24]. The vector potential only is introduced by the Peierls substitution [29]. Both represent $U(1)$ transformations in spinor space for which the local phase is introduced by a line integral. Therefore, we use a unified notation, whenever possible.

Definition 1: (Peierls and Schwinger substitution on the grid). The Peierls and Schwinger substitution for a spinor component $\psi = [u,v]$ on the grid are defined as follows [2,24,27,29]:

$$\psi^{t_j}_{x_j,y_j} \to \hat{\psi}^{t_j}_{x_j,y_j} = \exp\left\{-ia^{t_j}_{x_j,y_j}\right\}\psi^{t_j}_{x_j,y_j}. \tag{7}$$

(i) *Peierls substitution:* The real-valued phase $a^{t_j}_{x_j,y_j}$ is defined as the line integral of the vector potential $\mathcal{A}$ along $\mathbf{s}$ on time sheet t_j, starting at an arbitrary, but fixed position (x_o, y_o) and ending at the lattice point (x_j, y_j):

$$a^{t_j}_{x_j,y_j} = \frac{q}{\hbar c_o}\int_{(x_o,y_o)}^{(x,y)} d\mathbf{s}\cdot\mathcal{A}(\mathbf{s},t)|_{x=x_j,y=y_j,t=t_j}. \tag{8}$$

(ii) *Schwinger substitution:* The real-valued phase $a^{t_j}_{x_j,y_j}$ is defined as the line integral of the four-vector potential $(\mathcal{A},\Phi)$ along $(\mathbf{s},s_o)$ in four-vector space, starting at an arbitrary, but

fixed position (x_o, y_o, ct_o) and ending at (x_j, y_j, ct_j):

$$a^{t_j}_{x_j,y_j} = \frac{q}{\hbar c_o}\int_{(x_o,y_o,ct_o)}^{(x,y,ct)}\Big[d\mathbf{s}\cdot\mathcal{A}(\mathbf{s},s_o/c) - \frac{c_o}{c}ds_o\Phi(\mathbf{s},s_o/c)\Big]\Big|_{x=x_j,y=y_j,t=t_j}. \quad (9)$$

Note that Eq. (7) *per se* does not provide a "definition" of $\hat{\psi}$ since the phase resulting from the contour integral is path-dependent. This is not a problem in the continuum limit, since only local phase variations enter into the Dirac equation. The specific implementation of the integral on the grid will be discussed below. Both transformations represent a local phase-factor multiplication of the individual spinor components. There is no mixing of u and v components. The transformation is $U(1)$ on the entire grid but not in $2d$ spin space: there is no unique (local) pairing of u and v components: u and v occupy different grid sites. Since the basic scheme already accounts for the presence of a scalar potential, either of the two substitutions may be used to introduce the vector potential. However, there is a difference: the Schwinger substitution can introduce all four components of the electromagnetic potential in one sweep, while the Peierls substitution introduces the vector potential only.

A single-cone gauge-invariant numerical scheme for the dynamics of a Dirac fermion in general electromagnetic texture [Eq. (4)] is obtained by application of the single-cone scheme of Ref. [1] to the Peierls-Schwinger transformed spinor $\hat{\psi} = [\hat{u}, \hat{v}]$.

Definition 2: (Generalized single-cone finite difference scheme). The time-dependent Dirac equation Eq. (4) is approximated by the second-order accurate finite difference scheme for the Peierls, respectively, Schwinger transformed spinor $\hat{\psi} = [\hat{u}, \hat{v}]$, Definition 1, for $j_\nu \in \mathbb{Z}, \nu = o, x, y$:

$$\frac{\hat{u}^{j_o+\frac{1}{2}}_{j_x,j_y} - \hat{u}^{j_o-\frac{1}{2}}_{j_x,j_y}}{\Delta_o} = \left(\frac{m_z + \hat{V}}{i\hbar c}\right)^{j_o}_{j_x,j_y}\frac{\hat{u}^{j_o+\frac{1}{2}}_{j_x,j_y} + \hat{u}^{j_o-\frac{1}{2}}_{j_x,j_y}}{2} - \frac{\left(\hat{v}^{j_o}_{j_x,j_y+\frac{1}{2}} - \hat{v}^{j_o}_{j_x,j_y-\frac{1}{2}}\right)}{\Delta_y} - i\frac{\left(\hat{v}^{j_o}_{j_x+\frac{1}{2},j_y} - \hat{v}^{j_o}_{j_x-\frac{1}{2},j_y}\right)}{\Delta_x}, \quad (10)$$

$$\frac{\hat{u}^{j_o+\frac{1}{2}}_{j_x-\frac{1}{2},j_y-\frac{1}{2}} - \hat{u}^{j_o-\frac{1}{2}}_{j_x-\frac{1}{2},j_y-\frac{1}{2}}}{\Delta_o} = \left(\frac{m_z + \hat{V}}{i\hbar c}\right)^{j_o}_{j_x-\frac{1}{2},j_y-\frac{1}{2}}\frac{\hat{u}^{j_o+\frac{1}{2}}_{j_x-\frac{1}{2},j_y-\frac{1}{2}} + \hat{u}^{j_o-\frac{1}{2}}_{j_x-\frac{1}{2},j_y-\frac{1}{2}}}{2} - \frac{\left(\hat{v}^{j_o}_{j_x-\frac{1}{2},j_y} - \hat{v}^{j_o}_{j_x-\frac{1}{2},j_y-1}\right)}{\Delta_y} - i\frac{\left(\hat{v}^{j_o}_{j_x,j_y-\frac{1}{2}} - \hat{v}^{j_o}_{j_x-1,j_y-\frac{1}{2}}\right)}{\Delta_x}, \quad (11)$$

followed by

$$\frac{\hat{v}^{j_o+1}_{j_x-\frac{1}{2},j_y} - \hat{v}^{j_o}_{j_x-\frac{1}{2},j_y}}{\Delta_o} = \left(\frac{\hat{V} - m_z}{i\hbar c}\right)^{j_o+\frac{1}{2}}_{j_x-\frac{1}{2},j_y}\frac{\hat{v}^{j_o+1}_{j_x-\frac{1}{2},j_y} + \hat{v}^{j_o}_{j_x-\frac{1}{2},j_y}}{2} - \frac{\left(\hat{u}^{j_o+\frac{1}{2}}_{j_x-\frac{1}{2},j_y+\frac{1}{2}} - \hat{u}^{j_o+\frac{1}{2}}_{j_x-\frac{1}{2},j_y-\frac{1}{2}}\right)}{\Delta_y} + i\frac{\left(\hat{u}^{j_o+\frac{1}{2}}_{j_x,j_y} - \hat{u}^{j_o+\frac{1}{2}}_{j_x-1,j_y}\right)}{\Delta_x}, \quad (12)$$

and

$$\frac{\hat{v}^{j_o+1}_{j_x,j_y-\frac{1}{2}} - \hat{v}^{j_o}_{j_x,j_y-\frac{1}{2}}}{\Delta_o} = \left(\frac{\hat{V} - m_z}{i\hbar c}\right)^{j_o+\frac{1}{2}}_{j_x,j_y-\frac{1}{2}}\frac{\hat{v}^{j_o+1}_{j_x,j_y-\frac{1}{2}} + \hat{v}^{j_o}_{j_x,j_y-\frac{1}{2}}}{2} - \frac{\left(\hat{u}^{j_o+\frac{1}{2}}_{j_x,j_y} - \hat{u}^{j_o+\frac{1}{2}}_{j_x,j_y-1}\right)}{\Delta_y} + i\frac{\left(\hat{u}^{j_o+\frac{1}{2}}_{j_x+\frac{1}{2},j_y-\frac{1}{2}} - \hat{u}^{j_o+\frac{1}{2}}_{j_x-\frac{1}{2},j_y-\frac{1}{2}}\right)}{\Delta_x}. \quad (13)$$

Admitting integer and half-integer values for n, j, and k, $\hat{V}$ is defined as follows:

(i) For the Peierls substitution, introducing vector potential $\mathcal{A}$ and magnetization $(m_x, m_y, 0)$ only, one has

$$\hat{V}^n_{j,k} = V^n_{j,k} + \frac{q}{c_o}\int_{\mathbf{r}_o}^{\mathbf{r}} d\mathbf{s}\cdot\partial_t\mathcal{A}_{\text{eff}}(\mathbf{s},t)|_{x=x_j=j\Delta_x, y=y_j=k\Delta_y, t=t_j=n\Delta_t}. \quad (14)$$

Here

$$V^n_{j,k} = q\Phi^n_{j,k}$$

and

$$\mathcal{A}_{\text{eff}} = \begin{pmatrix}\mathcal{A}_x + \frac{c_o}{cq}m_y \\ \mathcal{A}_y - \frac{c_o}{cq}m_x\end{pmatrix}. \quad (15)$$

(ii) For a Schwinger substitution, introducing the complete electromagnetic potential $(\mathcal{A}, \Phi)$ and magnetization $(m_x, m_y, 0)$, one has

$$\hat{V}^n_{j,k} = 0. \quad (16)$$

(iii) For a Schwinger substitution, introducing the electromagnetic potential $(\mathcal{A}, 0)$ and magnetization $(m_x, m_y, 0)$, one has

$$\hat{V}^n_{j,k} = V^n_{j,k} = q\Phi^n_{j,k}. \quad (17)$$

For the Peierls substitution (i) one starts from the skeleton scheme with mass m_z and scalar potential term V; for a Schwinger substitution one may start with or without the presence of $V = q\Phi$, respectively, (iii) and (ii). In all cases, vector potential and in-plane magnetization can be introduced in one sweep.

B. Properties

For a discussion of the properties of this scheme, we define spatial difference operators as $(\delta_x f^{j_o})_{j_x,j_y} = f^{j_o}_{j_x+1/2,j_y} - f^{j_o}_{j_x-1/2,j_y}$ and $(\delta_y f^{j_o})_{j_x,j_y} = f^{j_o}_{j_x,j_y+1/2} - f^{j_o}_{j_x,j_y-1/2}$. Also, we define the inner product $(u^{j_o}, v^{j'_o})_{j'} := \sum_j u^{j_o}_j v^{j_o}_{j+j'} = \sum_j u^{j_o}_{j-j'} v^{*j'_o}_j$ on $l^2(\mathbb{Z}^2;\mathbb{C})$ and use the notation $\|u^{j_o}\|^2 := (u^{j_o}, u^{j_o})$, with the sum over j running over all lattice points on

time sheet j_o. Periodic or zero boundary conditions are used for the rectangular simulation domain. j' denotes a primitive displacement vector connecting the spatial sublattice of u with that of v.

Proposition 1. The properties of the scheme Eqs. (10) to (13) under periodic or zero boundary conditions may be summarized as follows:

(i) Let $r_x = \frac{\Delta_o}{\Delta_x}$, $r_y = \frac{\Delta_o}{\Delta_y}$. Then the functional

$$\begin{aligned} E^{j_o}_{r_x,r_y} &:= \|\hat{u}^{j_o+1/2}\|^2 + \|\hat{v}^{j_o+1}\|^2 \\ &\quad + \mathrm{Re}\{[(r_y\delta_y - i r_x\delta_x)\hat{u}^{j_o+1/2}, \hat{v}^{j_o+1}]\} \\ &= \text{const} = E^0_{r_x,r_y} \end{aligned} \tag{18}$$

is conserved under time propagation.

(ii) Let $r_x + r_y < 1$ (e.g., $r_x = r_y < 1/2$). Then the scheme Definition 2 is stable and satisfies the estimate

$$\|\hat{u}^{j_o+1/2}\|^2 + \|\hat{v}^{j_o+1}\|^2 \leqslant \frac{E^0_{r_x,r_y}}{1 - r_x - r_y}$$

for all time j_o.

(iii) Let $r = r_x = r_y = 1/\sqrt{2}$ hold in the scheme Definition 2. Furthermore, define a ("primed") norm

$$\begin{aligned} \left\|\hat{u}^{j_o-\frac{1}{2}}\right\|'^2 := \sum_{(j_x,j_y)} \Bigg| & \frac{\hat{u}^{j_o-\frac{1}{2}}_{j_x+\frac{1}{2},j_y+\frac{1}{2}} - i\hat{u}^{j_o-\frac{1}{2}}_{j_x+1,j_y}}{2\sqrt{2}} \\ & + \frac{\hat{u}^{j_o-\frac{1}{2}}_{j_x+\frac{1}{2},j_y-\frac{1}{2}} - i\hat{u}^{j_o-\frac{1}{2}}_{j_x,j_y}}{2\sqrt{2}} \Bigg|^2 \end{aligned} \tag{19}$$

and

$$\begin{aligned} \|\hat{v}^{j_o}\|'^2 := \sum_{(j_x,j_y)} \Bigg| & \frac{\hat{v}^{j_o}_{j_x,j_y+\frac{1}{2}} - i\hat{v}^{j_o}_{j_x+\frac{1}{2},j_y}}{2\sqrt{2}} \\ & + \frac{\hat{v}^{j_o}_{j_x,j_y-\frac{1}{2}} - i\hat{v}^{j_o}_{j_x-\frac{1}{2},j_y}}{2\sqrt{2}} \Bigg|^2, \end{aligned} \tag{20}$$

with $j_x, j_y \in \mathbb{Z}^2 \cup (\mathbb{Z} + 1/2)^2$.

Then the scheme Definition 2 is stable and satisfies for all time

$$\|\hat{u}\|'^2 + \|\hat{v}\|'^2 \leqslant 2E^0_{1/\sqrt{2},1/\sqrt{2}}.$$

Proof. The properties of scheme Definition 2 are a direct consequence of the properties of the underlying (2+1)-dimensional single-cone skeleton scheme of Ref. [1] and the fact that the Peierls-Schwinger substitution is a $U(1)$ symmetry operation on the grid. Hence the conserved functional in Eq. (18) for scheme Definition 2 is the Peierls-, respectively, Schwinger-transformed of the one for $\mathcal{A} = 0$. All stability conditions for r_x and r_y are preserved by the Peierls-Schwinger substitution. We note that the present formulation of the scheme uses the "physical" (i.e., TI) representation of the Dirac operator in Eq. (4). ■

Furthermore, the present scheme inherits scaling properties and second-order accuracy from the skeleton scheme. Higher-order accurate single-cone schemes can readily be devised and formulated on the staggered grid (Fig. 1) [30].

Proposition 2. The scheme of Definition 2 preserves gauge invariance on the lattice, *i.e.*, gauge invariance for the continuum formulation is carried over to the lattice formulation (Definition 2).

Proof. This property is a direct result of the construction of the scheme which first applies the Peierls-Schwinger substitution and then the discretization and placement on the staggered grid. ■

It is easy to verify that, within Schwinger and Peierls substitution, version (i), (ii), and (iii) of Definition 2, the scalar potential enters the scheme to within the same (second) order of accuracy.

IV. NUMERICAL IMPLEMENTATION AND APPROXIMATIONS

A. Formal scheme

The formal scheme Definition 2 [Eqs. (10) to (13)] under zero and periodic boundary conditions allows the construction of an exactly conserved functional leading to precise stability criteria. For numerical applications, however, the scheme is of limited direct use. In general the numerical value of the Peierls-Schwinger phase factors depends on the integration path. Moreover, in general, they are incompatible with periodic boundary conditions. These issues pose no problem when Eq. (7) is used in the evaluation of partial derivatives associated with the Dirac equation (4) since they merely require infinitesimal partial variations of the phase. On a grid, partial variations are finite in size. In particular, "equal time," u- and v-components and their (finite-difference approximations to) spatial derivatives live on adjacent time sheets.

Based on the formal scheme Definition 2, however, one can develop numerically tractable (approximate) schemes. Here we discuss four such schemes: (1) a scheme for static planar magnetic texture which conserves functional Eq. (18) exactly, (2) a single-update scheme, which conserves functional Eq. (18) for individual time steps, (3) a double update, and (4) a slowly varying-magnetic-field scheme. The latter two do not strictly conserve Eq. (18), but render the optimal time-resolution supported by the scheme. All four schemes support full time dependence of the scalar potential and mass (m_z) term. Due to the high Fermi velocity of Dirac fermions on TI surfaces, any physically relevant magnetic texture, in fact, will warrant a quasistatic or static treatment.

Expressing Eqs. (10) to (13) in terms of the spinor $\boldsymbol{\psi}$ with components u and v, one arrives at the formally exact implementation of the scheme arising from the Peierls-Schwinger substitution fulfilling Proposition 1 and 2. The formal scheme Definition 2 expressed in terms of the original spinor $[u,v]$ is lengthy and therefore is presented in the Appendix. However, it may be given a rather compact form. Permitting $j_\nu, \nu = 0,1,2$ to take integer and half-integer values, we define on the entire grid

$$(M_\pm)^{j_o}_{j_x,j_y} = \left(\frac{\hat{V} \pm m_z}{2i\hbar c}\right)^{j_o}_{j_x,j_y}. \tag{21}$$

Denoting the central grid point by ($j_o = j_x = j_y = 0$) and relative right or left shifts (by one half of the respective grid spacing) by $\pm$, one can solve for the final components $+$ in terms of the previous components $-$:

$$u^+_{0,0} = \frac{1}{e^{-i(a^+_{0,0}-a^0_{0,0})}\left(\frac{1}{\Delta_o} - M_+\right)^0_{0,0}}\left[\left(\frac{1}{\Delta_o} + M_+\right)^0_{0,0} e^{-i(a^-_{0,0}-a^0_{0,0})}u^-_{0,0} - \frac{e^{-i(a^0_{0,+}-a^0_{0,0})}v^0_{0,+} - e^{-i(a^0_{0,-}-a^0_{0,0})}v^0_{0,-}}{\Delta_y} - i\frac{e^{-i(a^0_{+,0}-a^0_{0,0})}v^0_{+,0} - e^{-i(a^0_{-,0}-a^0_{0,0})}v^0_{-,0}}{\Delta_x}\right], \tag{22}$$

followed by

$$v^+_{0,0} = \frac{1}{e^{-i(a^+_{0,0}-a^0_{0,0})}\left(\frac{1}{\Delta_o} - M_-\right)^0_{0,0}}\left[\left(\frac{1}{\Delta_o} + M_-\right)^0_{0,0} e^{-i(a^-_{0,0}-a^0_{0,0})}v^-_{0,0} - \frac{e^{-i(a^0_{0,+}-a^0_{0,0})}u^0_{0,+} - e^{-i(a^0_{0,-}-a^0_{0,0})}u^0_{0,-}}{\Delta_y} + i\frac{e^{-i(a^0_{+,0}-a^0_{0,0})}u^0_{+,0} - e^{-i(a^0_{-,0}-a^0_{0,0})}u^0_{-,0}}{\Delta_x}\right]. \tag{23}$$

As in the continuum case, only phases relative to the reference point enter. However, on the grid these variations are finite, and the reference points for u and v differ in time by $\Delta_t/2$. Since there are subtle differences between the use of the Peierls and the Schwinger substitution we shall discuss them separately.

B. Formal scheme based on the Peierls substitution

For a Peierls substitution, where time is a parameter, one is led to two types of relative phase factors. Spatial derivatives lead to a variation of the respective component of the endpoint of the integration path:

$$e^{-i(a^{j_o}_{j_x\pm\frac{1}{2},j_y} - a^{j_o}_{j_x,j_y})}, \quad e^{-i(a^{j_o}_{j_x,j_y\pm\frac{1}{2}} - a^{j_o}_{j_x,j_y})} \quad \text{(Type I)}. \tag{24}$$

This type can be computed locally and hence becomes independent from the integration path. The second type of phase factor is of the form

$$e^{-i(a^{j_o}_{j_x,j_y} - a^{j_o\pm\frac{1}{2}}_{j_x,j_y})} \quad \text{(Type II)}. \tag{25}$$

This phase corresponds to the line integral of $\partial_t \mathcal{A}$, suitably approximated on the grid, and as such remains path-dependent in general.[3] Such a contribution also enters in the correction to the scalar potential term according to Eq. (14). For time-independent vector potential, the Type II phase factor is 1, and one ends up with nontrivial phase factors of Type I only, well known from (time-independent) tight-binding and lattice QED models [3,7,31].

C. Formal scheme based on the Schwinger substitution

The Schwinger substitution treats space and time variables on equal footing. Partial variations of the phase Eq. (9) give

$$\delta a^t_{x,y} = \frac{q}{c_o\hbar}A_x(x,y,t)\delta_x, + \frac{q}{c_o\hbar}A_x(x,y,t)\delta_y - \frac{q}{\hbar}\Phi(x,y,t)\delta_t. \tag{26}$$

[3]Note that for this classification j_o, j_x, and j_y may take integer and half-integer values.

On the grid one may approximate as follows ($V = q\Phi$):

$$e^{-i(a^{j_o\pm\frac{1}{2}}_{j_x,j_y} - a^{j_o}_{j_x,j_y})} \approx e^{\pm i\frac{q\Delta_t}{4\hbar}((\Phi)^{j_o\pm\frac{1}{2}}_{j_x,j_y} + (\Phi)^{j_o}_{j_x,j_y})}, \tag{27}$$

$$e^{-i(a^{j_o}_{j_x\pm\frac{1}{2},j_y} - a^{j_o}_{j_x,j_y})} \approx e^{\mp i\frac{q\Delta_x}{4\hbar c_o}((\mathcal{A}_x)^{j_o}_{j_x\pm\frac{1}{2},j_y} + (\mathcal{A}_x)^{j_o}_{j_x,j_y})}, \tag{28}$$

$$e^{-i(a^{j_o}_{j_x,j_y\pm\frac{1}{2}} - a^{j_o}_{j_x,j_y})} \approx e^{\mp i\frac{q\Delta_y}{4\hbar c_o}((\mathcal{A}_y)^{j_o}_{j_x,j_y\pm\frac{1}{2}} + (\mathcal{A}_y)^{j_o}_{j_x,j_y})}. \tag{29}$$

Indeed, starting with m_z and V in their desired final form, a Schwinger substitution with $\Phi = 0$ provides the simplest method for implementation of the vector potential into the kinetic momentum [Eq. (2)] for the scheme Eqs. (22) and (23).

D. Time-independent x-y magnetic textures: Static scheme

For the case of time-independent planar magnetic texture there are no corrections to the scalar potential term from the Peierls substitution. The Type II phase factors in Eqs. (22) and (23) are equal to one. Schwinger and Peierls substitution give identical results since Type I phase factors may be approximated by Eqs. (28) and (29). The symmetric choice in the lattice-discretization allows the use of periodic boundary conditions and yields conservation of functional $E^{j_o}_{r_x,r_y}$ in Eq. (18) within consistent discretization. It takes the form

$$E^{j_o}_{r_x,r_y} := \|u^{j_o+1/2}\|^2 + \|v^{j_o+1}\|^2 + \mathrm{Re}[((r_yD_y - ir_xD_x)u^{j_o+1/2}, v^{j_o+1})], \tag{30}$$

where difference operators D_x and D_y are defined on the barred grids and act on spinor components ψ according to

$$D_x\psi^{j_o}_{j_x,j_y} = e^{-i\frac{q\Delta_x}{4\hbar c_o}\left[(\mathcal{A}_x)^{j_o}_{j_x+\frac{1}{2},j_y} + (\mathcal{A}_x)^{j_o}_{j_x,j_y}\right]}\psi^{j_o}_{j_x+\frac{1}{2},j_y} - e^{i\frac{q\Delta_x}{4\hbar c_o}\left[(\mathcal{A}_x)^{j_o}_{j_x-\frac{1}{2},j_y} + (\mathcal{A}_x)^{j_o}_{j_x,j_y}\right]}\psi^{j_o}_{j_x-\frac{1}{2},j_y}, \tag{31}$$

$$D_y\psi^{j_o}_{j_x,j_y} = e^{-i\frac{q\Delta_y}{4\hbar c_o}\left[(\mathcal{A}_y)^{j_o}_{j_x,j_y+\frac{1}{2}} + (\mathcal{A}_y)^{j_o}_{j_x,j_y}\right]}\psi^{j_o}_{j_x,j_y+\frac{1}{2}} - e^{i\frac{q\Delta_y}{4\hbar c_o}\left[(\mathcal{A}_y)^{j_o}_{j_x,j_y} + (\mathcal{A}_y)^{j_o}_{j_x,j_y-\frac{1}{2}}\right]}\psi^{j_o}_{j_x,j_y-\frac{1}{2}}. \tag{32}$$

Propositions 1 and 2 apply.

E. Time-dependent x-y magnetic textures

For the case of space- and time-dependent x-y magnetic textures one best introduces the vector potential $\mathcal{A}(x,y,t)$ by a Schwinger substitution with $m_z(x,y,t)$ and $V(x,y,t)$ present in the skeleton scheme, i.e., version (iii) of Definition 2. This leaves one with Type I phase factors. From the explicit form of the scheme, with u- and v-components located on different time sheets, it is readily seen that a lattice implementation of the Schwinger (Peierls) substitution based on relative phases leads to approximations which will not support exact conservation of functional Eq. (18). For example, in the partial y-derivatives of Eq. (22) one has terms $\exp\{-i(a^0_{0,\pm} - a^0_{0,0})\} = \exp\{-i(a^{j_o}_{j_x,j_y\pm\frac{1}{2}} - a^{j_o}_{j_x,j_y})\}$; however, $\exp\{-i(a^0_{0,\pm} - a^0_{0,0})\} = \exp\{-i(a^{j_o+\frac{1}{2}}_{j_x+\frac{1}{2},j_y\pm\frac{1}{2}} - a^{j_o+\frac{1}{2}}_{j_x+\frac{1}{2},j_y})\}$ in Eq. (23). Within approximations Eqs. (28) and (29) this time shift prohibits the simple integration by parts rule which allows the elimination of mixed-time terms leading to the conservation of functional Eq. (18). This can be remedied by an average over time j_o and $j_o+\frac{1}{2}$, leading to the single-update scheme below. Alternatively, one can accept nonconservation of functional Eq. (18) on the grid and use two sets of phase factors: one for the u update from time $j_o-\frac{1}{2}$ to $j_o+\frac{1}{2}$, and one set for the v update from time j_o to j_o+1. The natural choice for average time, respectively, is j_o and $j_o+\frac{1}{2}$. This will be the double-update scheme below. For slowly varying x-y magnetic textures, the phase factors may be linearized in $\mathcal{A}(x,y,t)$. This leads to a slowly varying-magnetic-field approximation of the scheme.

The computation of the conserved functional expressed in terms of u and v too entails a numerical approximation of relative phase factors in the inner product between u- and v-components in the third term on the r.h.s. of Eq. (18). For the summation-by-parts rule for the inner product between $\hat{u}^{j_o+\frac{1}{2}}$ and $\hat{v}^{j_o}$ to hold in a numerical implementation, in Eq. (18) one needs to introduce time-averaged relative phase factors, such as

$$e^{-i\left(a^{j_o+1}_{j_x\pm\frac{1}{2},j_y} - a^{j_o+\frac{1}{2}}_{j_x,j_y}\right)} \approx e^{\mp i\frac{q\Delta_x}{8\hbar c_o}\left[(\mathcal{A}_x)^{j_o+1}_{j_x\pm\frac{1}{2},j_y} + (\mathcal{A}_x)^{j_o+1}_{j_x,j_y} + (\mathcal{A}_x)^{j_o+\frac{1}{2}}_{j_x\pm\frac{1}{2},j_y} + (\mathcal{A}_x)^{j_o+\frac{1}{2}}_{j_x,j_y}\right]}, \quad (33)$$

$$e^{-i\left(a^{j_o+1}_{j_x,j_y\pm\frac{1}{2}} - a^{j_o+\frac{1}{2}}_{j_x,j_y}\right)} \approx e^{\mp i\frac{q\Delta_y}{8\hbar c_o}\left[(\mathcal{A}_y)^{j_o+1}_{j_x,j_y\pm\frac{1}{2}} + (\mathcal{A}_y)^{j_o+1}_{j_x,j_y} + (\mathcal{A}_y)^{j_o+\frac{1}{2}}_{j_x,j_y\pm\frac{1}{2}} + (\mathcal{A}_y)^{j_o+\frac{1}{2}}_{j_x,j_y}\right]}. \quad (34)$$

F. Single-update scheme

Time-dependent x-y magnetic textures can be accounted for by a slight modification of the static scheme in which the x-y magnetic texture is kept time-independent during a single u-v update under Eqs. (22) and (23) (spinor propagation by one time step) and is updated prior to the next time step. Type II phase factors then are equal to one, and the correction term to the scalar potential Eq. (14) is zero for both Peierls and Schwinger substitution. This scheme preserves the functional Eq. (30) during a single execution of Eqs. (22) and (23), but needs to be updated in preparation for the next iteration. In summary, the scheme works as follows:

(1) Update the Type I relative phase factors according to Eqs. (33) and (34), averaging over time j_o and $j_o+\frac{1}{2}$. Use them to update functional Eq. (30).

(2) Execute scheme Eq. (22) followed by Eq. (23) (Type II phase factors set equal to one), thereby conserving Eq. (30).

(3) Increase $j_o \to j_o+1$ and go back to step 1, or terminate when final time is reached.

The change of functional Eq. (30) due to the update ($-$: before update, $+$: after update at time $j_o+\frac{1}{2}, j_o+1$) of the phase factor can readily be estimated to be

$$\left|\left(E^{j_o}_{r_x,r_y}\right)^+ - \left(E^{j_o}_{r_x,r_y}\right)^-\right| \leqslant 2(r_x+r_y)(\|u^{j_o+1/2}\|^2 + \|v^{j_o+1}\|^2).$$

G. Double-update scheme

A better time resolution is achieved by a double-update of the Type I phase factors (with Type II phase factors equal to one) according to the following procedure:

(1) Update the Type I relative phase factors in Eqs. (28) and (29) to the values at time j_o.

(2) Execute Eq. (22) to propagate $u^{j_0-1/2}$ to $u^{j_0+1/2}$.

(3) Update the Type I relative phase factors in Eqs. (28) and (29) to the values at time $j_o+1/2$.

(4) Execute Eq. (23) to propagate v^{j_0} to v^{j_0+1}.

(5) Increase $j_o \to j_o+1$ and go back to step 1 or terminate when final time is reached.

This scheme does not strictly conserve functional Eqs. (18) or (30).

H. Slowly varying magnetic-field scheme

For smooth space-time variations of the in-plane texture, the formal scheme Eqs. (A3) to (A6) may be simplified by using the approximations Eqs. (A1) and (A2) given in the Appendix. f_- terms may be dropped, difference quotients of exponentials may be approximated, and the remaining factors f_+ all may be set equal and canceled out of the respective equation. For the Peierls substitution, one arrives at the greatly simplified form (slowly varying-magnetic-field scheme)

$$\begin{aligned}\frac{\left(u^{j_o+\frac{1}{2}}_{j_x,j_y} - u^{j_o-\frac{1}{2}}_{j_x,j_y}\right)}{\Delta_o} = &\left[\left(\frac{m_z+\hat{V}}{i\hbar c}\right)^{j_o}_{j_x,j_y} + i\frac{\left(a^{j_o+\frac{1}{2}}_{j_x,j_y} - a^{j_o-\frac{1}{2}}_{j_x,j_y}\right)}{\Delta_o}\right]\frac{\left(u^{j_o+\frac{1}{2}}_{j_x,j_y} + u^{j_o-\frac{1}{2}}_{j_x,j_y}\right)}{2}\\ &-\left[\frac{\left(v^{j_o}_{j_x,j_y+\frac{1}{2}} - v^{j_o}_{j_x,j_y-\frac{1}{2}}\right)}{\Delta_y} - i\frac{\left(a^{j_o}_{j_x,j_y+\frac{1}{2}} - a^{j_o}_{j_x,j_y-\frac{1}{2}}\right)}{\Delta_y}\frac{\left(v^{j_o}_{j_x,j_y+\frac{1}{2}} + v^{j_o}_{j_x,j_y-\frac{1}{2}}\right)}{2}\right]\\ &-i\left[\frac{\left(v^{j_o}_{j_x+\frac{1}{2},j_y} - v^{j_o}_{j_x-\frac{1}{2},j_y}\right)}{\Delta_x} - i\frac{\left(a^{j_o}_{j_x+\frac{1}{2},j_y} - a^{j_o}_{j_x-\frac{1}{2},j_y}\right)}{\Delta_x}\frac{\left(v^{j_o}_{j_x+\frac{1}{2},j_y} + v^{j_o}_{j_x-\frac{1}{2},j_y}\right)}{2}\right],\end{aligned} \quad (35)$$

$$\frac{\left(u^{j_o+\frac{1}{2}}_{j_x-\frac{1}{2},j_y-\frac{1}{2}}-u^{j_o-\frac{1}{2}}_{j_x-\frac{1}{2},j_y-\frac{1}{2}}\right)}{\Delta_o}=\left[\left(\frac{m_z+\hat{V}}{i\hbar c}\right)^{j_o}_{j_x-\frac{1}{2},j_y-\frac{1}{2}}+i\frac{\left(a^{j_o+\frac{1}{2}}_{j_x-\frac{1}{2},j_y-\frac{1}{2}}-a^{j_o-\frac{1}{2}}_{j_x-\frac{1}{2},j_y-\frac{1}{2}}\right)}{\Delta_o}\right]\frac{\left(u^{j_o+\frac{1}{2}}_{j_x-\frac{1}{2},j_y-\frac{1}{2}}+u^{j_o-\frac{1}{2}}_{j_x-\frac{1}{2},j_y-\frac{1}{2}}\right)}{2}$$
$$-\left[\frac{\left(v^{j_o}_{j_x-\frac{1}{2},j_y}-v^{j_o}_{j_x-\frac{1}{2},j_y-1}\right)}{\Delta_y}-i\frac{\left(a^{j_o}_{j_x-\frac{1}{2},j_y}-a^{j_o}_{j_x-\frac{1}{2},j_y-1}\right)}{\Delta_y}\frac{\left(v^{j_o}_{j_x-\frac{1}{2},j_y}+v^{j_o}_{j_x-\frac{1}{2},j_y-1}\right)}{2}\right]$$
$$-i\left[\frac{\left(v^{j_o}_{j_x,j_y-\frac{1}{2}}-v^{j_o}_{j_x-1,j_y-\frac{1}{2}}\right)}{\Delta_x}-i\frac{\left(a^{j_o}_{j_x,j_y-\frac{1}{2}}-a^{j_o}_{j_x-1,j_y-\frac{1}{2}}\right)}{\Delta_x}\frac{\left(v^{j_o}_{j_x,j_y-\frac{1}{2}}+v^{j_o}_{j_x-1,j_y-\frac{1}{2}}\right)}{2}\right], \tag{36}$$

followed by

$$\frac{\left(v^{j_o+1}_{j_x-\frac{1}{2},j_y}-v^{j_o}_{j_x-\frac{1}{2},j_y}\right)}{\Delta_o}=\left[\left(\frac{\hat{V}-m_z}{i\hbar c}\right)^{j_o+\frac{1}{2}}_{j_x-\frac{1}{2},j_y}+i\frac{\left(a^{j_o+1}_{j_x-\frac{1}{2},j_y}-a^{j_o}_{j_x-\frac{1}{2},j_y}\right)}{\Delta_o}\right]\frac{\left(v^{j_o+1}_{j_x-\frac{1}{2},j_y}+v^{j_o}_{j_x-\frac{1}{2},j_y}\right)}{2}$$
$$-\left[\frac{\left(u^{j_o+\frac{1}{2}}_{j_x-\frac{1}{2},j_y+\frac{1}{2}}-u^{j_o+\frac{1}{2}}_{j_x-\frac{1}{2},j_y-\frac{1}{2}}\right)}{\Delta_y}-i\frac{\left(a^{j_o+\frac{1}{2}}_{j_x-\frac{1}{2},j_y+\frac{1}{2}}-a^{j_o+\frac{1}{2}}_{j_x-\frac{1}{2},j_y-\frac{1}{2}}\right)}{\Delta_y}\frac{\left(u^{j_o+\frac{1}{2}}_{j_x-\frac{1}{2},j_y+\frac{1}{2}}+u^{j_o+\frac{1}{2}}_{j_x-\frac{1}{2},j_y-\frac{1}{2}}\right)}{2}\right]$$
$$+i\left[\frac{\left(u^{j_o+\frac{1}{2}}_{j_x,j_y}-u^{j_o+\frac{1}{2}}_{j_x-1,j_y}\right)}{\Delta_x}-i\frac{\left(a^{j_o+\frac{1}{2}}_{j_x,j_y}-a^{j_o+\frac{1}{2}}_{j_x-1,j_y}\right)}{\Delta_x}\frac{\left(u^{j_o+\frac{1}{2}}_{j_x,j_y}+u^{j_o+\frac{1}{2}}_{j_x-1,j_y}\right)}{2}\right] \tag{37}$$

and

$$\frac{\left(v^{j_o+1}_{j_x,j_y-\frac{1}{2}}-v^{j_o}_{j_x,j_y-\frac{1}{2}}\right)}{\Delta_o}=+\left[\left(\frac{\hat{V}-m_z}{i\hbar c}\right)^{j_o+\frac{1}{2}}_{j_x,j_y-\frac{1}{2}}+i\frac{\left(a^{j_o+1}_{j_x,j_y-\frac{1}{2}}-a^{j_o}_{j_x,j_y-\frac{1}{2}}\right)}{\Delta_o}\right]\frac{\left(v^{j_o+1}_{j_x,j_y-\frac{1}{2}}+v^{j_o}_{j_x,j_y-\frac{1}{2}}\right)}{2}$$
$$-\left[\frac{\left(u^{j_o+\frac{1}{2}}_{j_x,j_y}-u^{j_o+\frac{1}{2}}_{j_x,j_y-1}\right)}{\Delta_y}-i\frac{\left(a^{j_o+\frac{1}{2}}_{j_x,j_y}-a^{j_o+\frac{1}{2}}_{j_x,j_y-1}\right)}{\Delta_y}\frac{\left(u^{j_o+\frac{1}{2}}_{j_x,j_y}+u^{j_o+\frac{1}{2}}_{j_x,j_y-1}\right)}{2}\right]$$
$$+i\left[\frac{\left(u^{j_o+\frac{1}{2}}_{j_x+\frac{1}{2},j_y-\frac{1}{2}}-u^{j_o+\frac{1}{2}}_{j_x-\frac{1}{2},j_y-\frac{1}{2}}\right)}{\Delta_x}-i\frac{\left(a^{j_o+\frac{1}{2}}_{j_x+\frac{1}{2},j_y-\frac{1}{2}}-a^{j_o+\frac{1}{2}}_{j_x-\frac{1}{2},j_y-\frac{1}{2}}\right)}{\Delta_x}\frac{\left(u^{j_o+\frac{1}{2}}_{j_x+\frac{1}{2},j_y-\frac{1}{2}}+u^{j_o+\frac{1}{2}}_{j_x-\frac{1}{2},j_y-\frac{1}{2}}\right)}{2}\right]. \tag{38}$$

These equations explicitly reveal the presence of the vector potential in the Dirac Hamiltonian in two positions. There is a correction to the scalar potential from $\hat{V}^{j_o}_{j_x,j_y}$ back to the physical scalar potential

$$V^n_{j,k}=\hat{V}^n_{j,k}-\frac{q}{c_o}\int^{(x,y)}_{(x_o,y_o)}d\mathbf{s}\cdot\left.\frac{\mathcal{A}(\mathbf{s},t)|_{t=\Delta_t(n+\frac{1}{2})}-\mathcal{A}(\mathbf{s},t)|_{t=\Delta_t(n-\frac{1}{2})}}{\Delta t}\right|_{x=\Delta_x j,y=\Delta_y k} \tag{39}$$

consistent with the electric field [32–34]. Note that $V^n_{j,k}=q\,\Phi^n_{j,k}$.

Under the Peierls substitution, the spatial j-derivative term transforms according to

$$\frac{\psi_{j+\frac{1}{2}}-\psi_{j-\frac{1}{2}}}{\Delta_j}\to\frac{\psi_{j+\frac{1}{2}}-\psi_{j-\frac{1}{2}}}{\Delta_j}-\frac{iq}{\hbar c_o}\mathcal{A}_j\frac{\psi_{j+\frac{1}{2}}+\psi_{j-\frac{1}{2}}}{2},\qquad j=x,y,$$

which represents the "minimal-gauge" introduction of the vector potential into the kinetic momentum vector $\mathbf{\Pi}$ [Eq. (2)] consistent with the grid and the presence of a magnetic field and/or magnetic texture [32,33]. The proper placement of terms containing x and y components of the magnetization follows from the placement of the vector potential y and x components, respectively,

$$(m_x)^n_{j,k}\sim-\hbar c\frac{a^n_{j,k+\frac{1}{2}}-a^n_{j,k-\frac{1}{2}}}{\Delta y}\approx-\frac{qc}{c_o}(\mathcal{A}_y)^n_{j,k}, \tag{40}$$

$$(m_y)^n_{j,k}\sim\hbar c\frac{a^n_{j+\frac{1}{2},k}-a^n_{j-\frac{1}{2},k}}{\Delta x}\approx\frac{qc}{c_o}(\mathcal{A}_x)^n_{j,k}. \tag{41}$$

Using centered derivatives over single lattice spacings only, this approximate scheme still is based on a single Dirac cone dispersion. It offers an intuitive finite-difference discretization scheme for the underlying continuum equation Eq. (4) and eliminates the need for a calculation of phase factors. However,

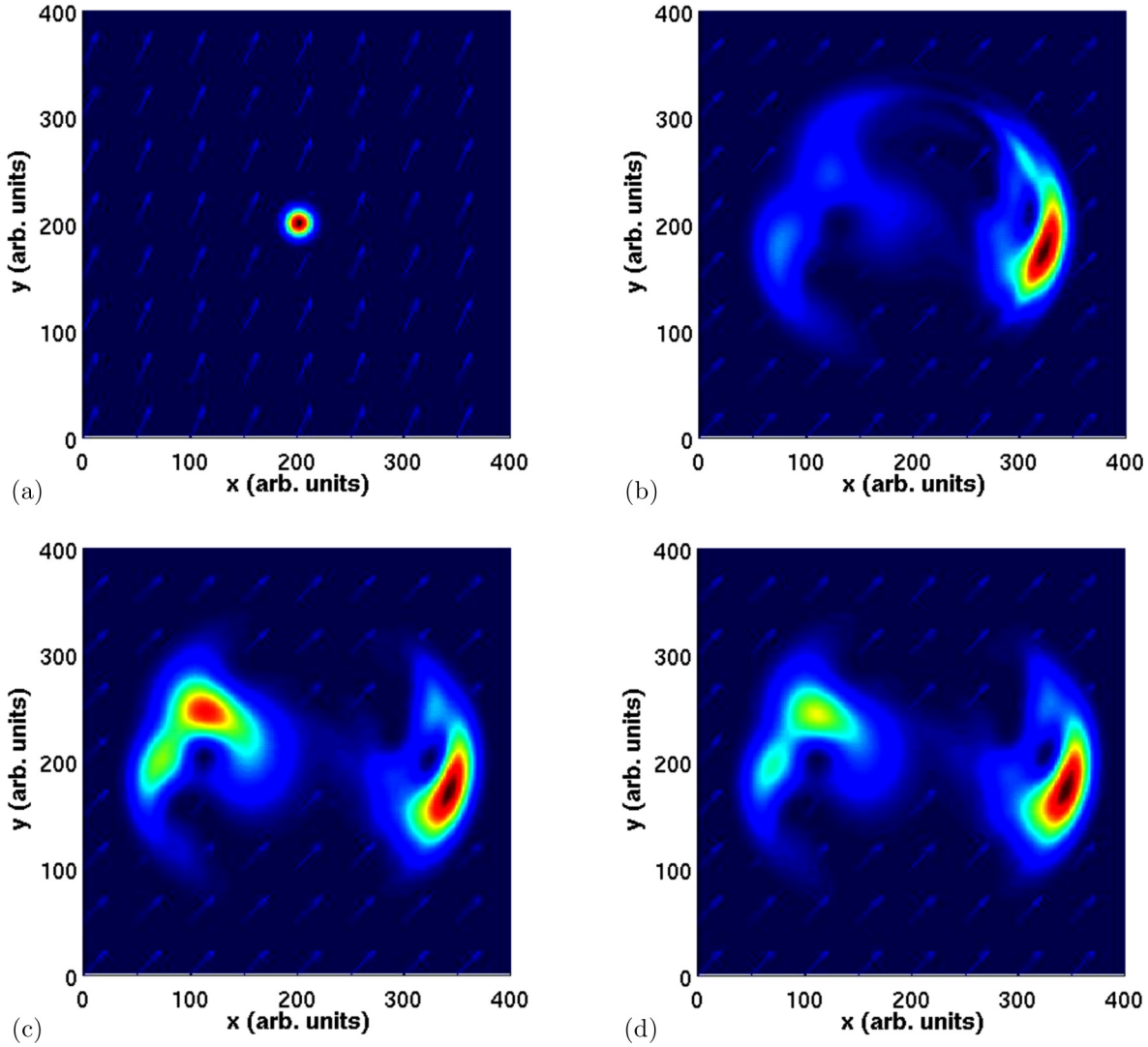

FIG. 2. Dirac fermion propagation across a region of rotating uniform magnetization $m_0 = 0.02\,\text{eV}$, $\omega = 0.05 \times 2\pi/\Delta_t = 5.5 \times 10^{13}\,\text{Hz}$: (a) particle density of the initial Gaussian wave packet placed at the center of the simulation region; particle density after 180 time steps (1 fs) within (b) the formal scheme (Peierls substitution), (c) the single-update scheme, and (d) the slowly varying-magnetic-field scheme [Eqs. (35)–(38)]. Magnetic texture is indicated by arrows.

a conserved functional, such as Eqs. (18) or (30), has not been identified.

V. NUMERICAL EXAMPLES

For basic numerical testing of stability and convergence of the proposed numerical schemes we confine ourselves to in-plane magnetization texture. Stability for the case of time-dependent external scalar potential and mass-term (m_z) has been demonstrated [1,23]. For the numerical simulations we choose a rectangular region of typically 1000 nm by 1000 nm and at least 250×250 mesh points per time sheet pair. Periodic boundary conditions are applied for the purpose of stability testing. In transport simulations absorbing boundary layers may be added upon demand. Parameters typical for TIs are used; e.g., the Fermi velocity is set to $c = 6.2\times10^5$ m/s and the effective magnetization energy is of the order of several tens of meV. The mass term m_z is set equal to zero.

For starting a simulation the spinor at initial time t_o must be placed onto two adjacent time sheets of the grid, e.g., $j_o - 1/2$ and j_o; see Fig. 1. One may proceed as follows: Put the v-component onto the v-type fcc time sheet j_o. Place the u-component onto a u-type fcc time sheet and use v and the fields at time j_o to propagate u back in time by half a time step onto time sheet $j_o - 1/2$. Now start with the simulation by propagating u from $j_o - 1/2$ to $j_o + 1/2$, followed by v from j_o to $j_o + 1$, and so on.

A. Rotating in-plane magnetization

For a first example, we consider a time-dependent spatially uniform magnetization rotating in the x-y plane

$$\mathbf{m}(x,y,t) = \big(m_x^0 \cos(\omega t + \phi), m_y^0 \sin(\omega t + \phi)\big).$$

Since the associated Peierls phase is path-independent, this system allows a numerical treatment within the formal scheme

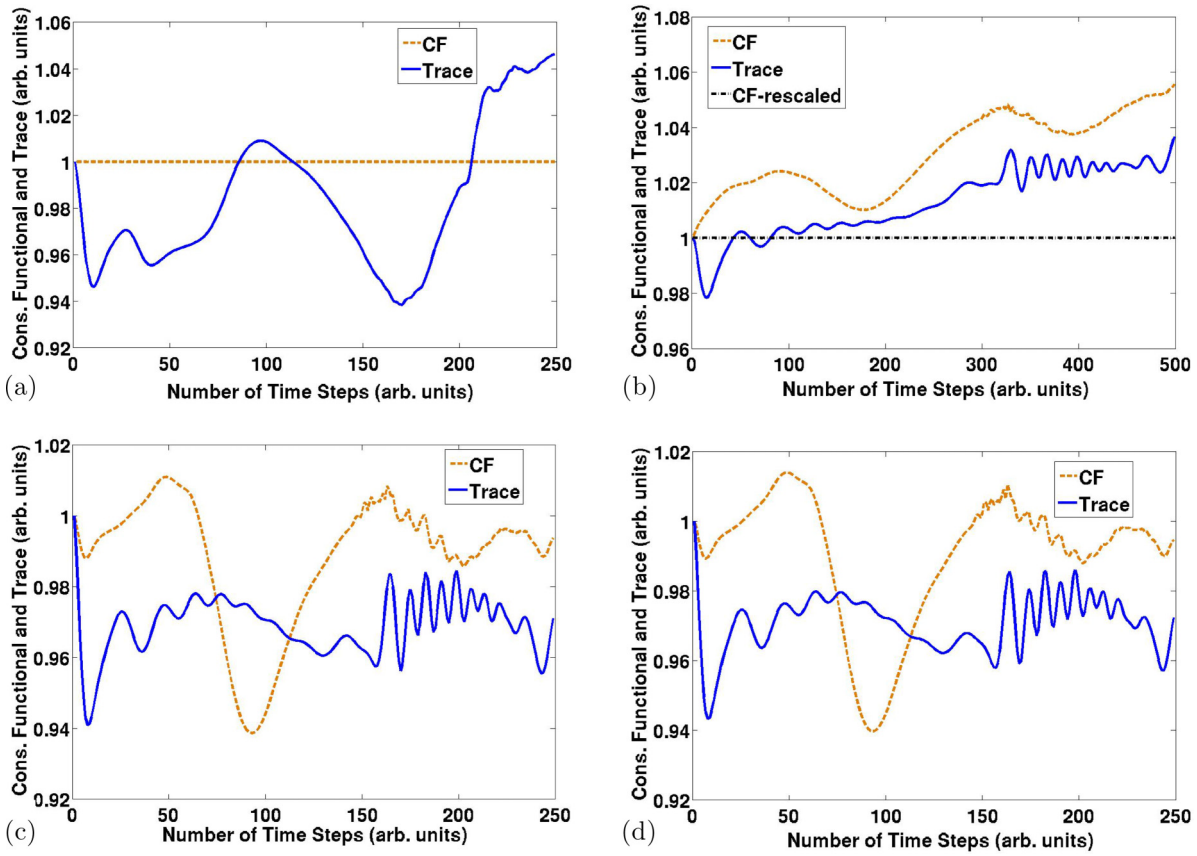

FIG. 3. Conserved functional (CF) [Eq. 18] (dashed line) and lattice trace (solid line) for the simulation of a Dirac fermion propagation across a region of rotating uniform magnetization $m_0 = 0.02\,\mathrm{eV}$, $\omega = 0.05\times 2\pi/\Delta_t = 5.5\times 10^{13}$ Hz: (a) formal scheme (Peierls transformation), (b) single-update scheme, (c) double-update scheme, and (d) slowly varying-magnetic-field scheme Eqs. (35)–(38).

Definition 2 (i). Conservation of functional Eq. (18), evaluated on the grid, must be fulfilled. This allows a direct comparison with the approximate schemes. Still, the path integral over the time derivative of the vector potential [Eq. (14)] does not support periodic boundary conditions on physical grounds. For testing purposes, however, they are enforced on the Peierls transformed spinor.

The Peierls phase factor is computed as follows. The lower left corner of the rectangular simulation region is the starting point (j_{x_o}, j_{y_o}) of the path which, in increments of $\Delta_x/2$, first leads along the lower edge of the simulation region to position (j_x, j_{y_o}), and then in increments of $\Delta_y/2$ vertically up to position (j_x, j_y):

$$\int_{(x_o,y_o)}^{(x,y)} d\mathbf{s}\cdot\mathcal{A}(\mathbf{s},t)|_{x=x_j,y=y_j,t=t_j} \approx \frac{1}{4}\left\{\Delta_x \sum_{n=1}^{2(j_x-j_{x_o})}\left[(\mathcal{A}_x)^{t_j}_{j_{x_o}+\frac{n}{2},j_{y_o}} + (\mathcal{A}_x)^{t_j}_{j_{x_o}+\frac{n-1}{2},j_{y_o}}\right] + \Delta_y \sum_{n=1}^{2(j_y-j_{y_o})}\left[(\mathcal{A}_y)^{t_j}_{j_x,j_{y_o}+\frac{n}{2}} + (\mathcal{A}_y)^{t_j}_{j_x,j_{y_o}+\frac{n-1}{2}}\right]\right\}. \quad (42)$$

Other path choices for computation of the phase of the Type II phase factors are permissible, as long as they are consistent with the relative phase factors Type I and the implementation of the correction term to the scalar potential.

A Gaussian wave packet with $m_z = 0$, average kinetic energy 10 meV, and initial central wave vector in the x direction is released in the center of a 1 μm × 1 μm simulation region. Here 400×400 mesh points are used for a pair of u-v time sheets, which corresponds to $\Delta = \Delta_x = \Delta_y = 0.5\times 10^{-8}$ m. The simulation of a wave packet propagation from the center of the simulation region towards the boundaries of the simulation region is performed within each of the time-dependent schemes. Each simulation consists of 250 iterations using the time step $\Delta_t = \Delta/(c\sqrt{2}) = 0.57\times 10^{-14}$ s. The latter represents the maximum permissible time step to ensure stability within the formal scheme Definition 2. The effective magnetization vector of magnitude 20 meV rotates with angular frequency $\omega = 0.05$, in units of inverse Δ_t, corresponding to 5.5×10^{14} Hz. An initial phase $\phi = \pi/3$ is used.[4]

Figure 2(a) gives a top view of the probability density of the wave packet upon its release. The in-plane magnetization direction is indicated by (blue) arrows. Figures 2(b)–2(d) give the wave packet after approximately 180 iterations (corresponding to a 150° rotation of the magnetization vector),

[4]Here parameters are chosen deliberately to provoke differences in the results within different approximations.

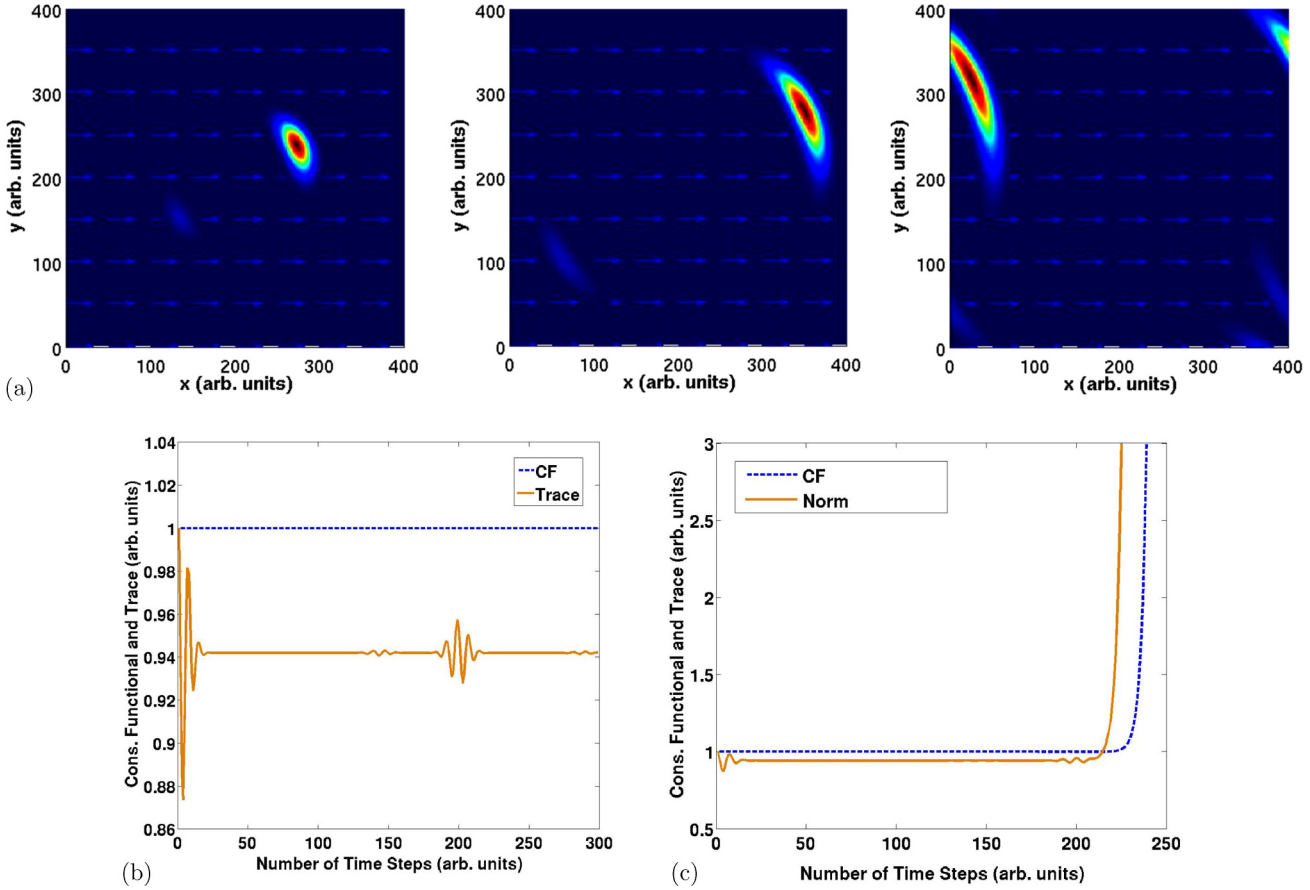

FIG. 4. Dirac fermion propagation across a region of constant magnetization $m_x = 0.02\,\mathrm{eV}, m_y = m_z = 0$: (a) three snap shots of the particle density evolving from a Gaussian wave packet initially placed at the center of the simulation region; conserved functional Eq. (18) (dashed line) and lattice norm (solid line) for the simulations: (b) within the formal scheme (Peierls substitution), (c) within the slowly varying-magnetic-field scheme [Eqs. (35)–(38)].

respectively, within the formal, the single update, and the slowly varying-magnetic-field scheme [Eqs. (35)–(38)]. Differences in the numerical results within the three schemes are evident, and they have several origins. The formal scheme implements periodic boundary conditions. While allowing a stability estimate for this scheme, they are not compatible with a uniform rotating magnetization vector near the simulation boundaries. Effects are apparent already after 180 time steps due to the rapid propagation of the wave packet towards the simulation boundaries. The formal, double update (results not shown here), and the slowly varying-magnetic-field scheme update the magnetic texture both for the u and v update and hence have twice as fine a time resolution as the single-update scheme. Note that here the goal is not to obtain an accurate simulation of the time evolution but rather, using the maximum permissible time step, to explore stability under the different schemes.[5] The double-update scheme is found to give results which, at time step 180, are practically identical to those within the slowly varying magnetization scheme [Fig. 2(d)]. For longer simulation time one finds that the formal scheme has essential spurious contributions from the (artificial) periodic boundary conditions. Moreover, the slowly varying-magnetic-field scheme has less favorable stability properties than the formal, single-, and double-update scheme, as will be discussed below.

Figures 3(a)–3(d), respectively, give the (conserved) functional Eq. (30) and the trace for the formal, single-update, double-update, and slowly varying-magnetic-field scheme. All four schemes remain stable throughout the 250 time steps of the simulation. The trace, shown as a continuous blue line, is defined as the lattice sum of diagonal elements of u-v time sheet pairs. It is not conserved but is found to deviate not too much from its initial value. This is typical under stable behavior. Main differences occur in the evolution of the "conserved functional" Eq. (18) [respectively Eq. (30)]. It can be seen in Fig. 3(a) that conservation of Eq. (18) for the formal scheme is confirmed. Figure 3(b) shows the result for the single-update scheme. At the maximum time step compatible with stability, the rapid rotation of the magnetization is captured somewhat poorly. Functional Eq. (30) is found to rise in an oscillatory fashion for the duration of the simulation. During a single time-step iteration functional Eq. (30) is conserved: The dashed-dotted line, showing the ratio of Eq. (30) after and prior to the propagation by a single time step, stays constant at value one. Note that functional Eq. (30) is not equal to functional (18). Figure 3(c) gives the result

[5]Stability clearly is not the sole criterium for choosing the time step when dealing with time-dependent textures.

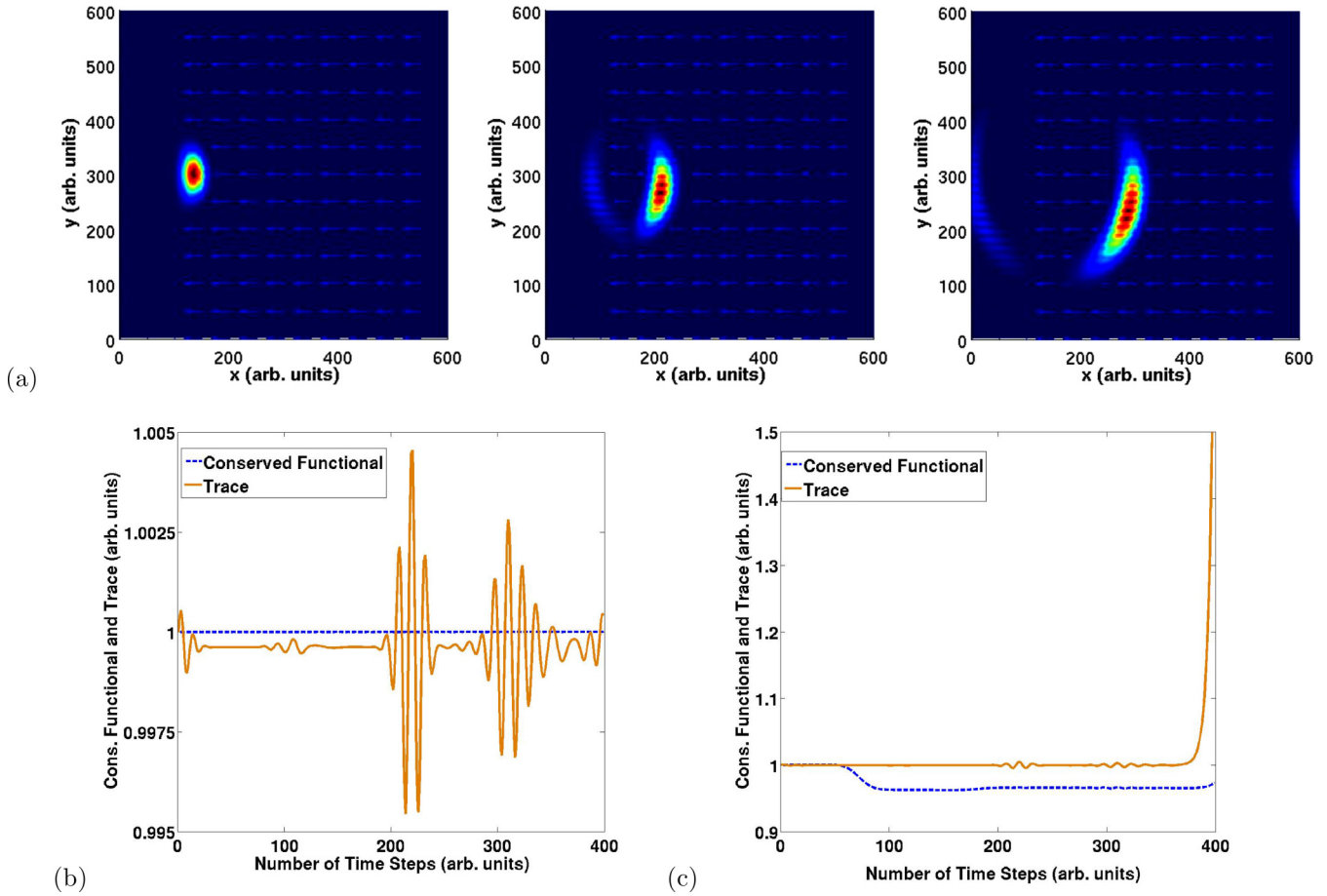

FIG. 5. Dirac fermion scattering at a magnetization step $m_x = -0.02\,\mathrm{eV}$, $m_y = m_z = 0$ under normal incidence: (a) three snapshots of the particle density evolving from a Gaussian wave packet initially placed at the center of the simulation region; conserved functional (30) (dashed line) and trace (lattice norm) (solid line) for the simulations: (b) within the formal scheme (Peierls substitution), (c) within the slowly varying-magnetic-field scheme [Eqs. (35)–(38)].

for the double-update scheme, in which the Type I phase factors are updated after every u- and v-propagation. This scheme clearly gives a better time resolution than the adiabatic scheme but does not leave invariant functional Eq. (30) [or (18)] during a single-time-step u-v progression. Long-term variation of functional Eq. (30), however, is smaller than for the single-update scheme. As for the probability density above, results compare very well with the ones obtained within the scheme for slowly varying in-plane texture, shown in Fig. 3(d): oscillatory behavior is found for the functional Eq. (30). However, as will be shown for examples below, long-term stability of the latter scheme is not ensured.

B. Static in-plane magnetization

Static in-plane magnetization, in conjunction with general time-dependent scalar potential and mass terms, allows a numerical implementation of the scheme Definition 2 which leads to conservation of functional Eq. (30), derived from (18). Propositions 1 and 2 hold. We start with a constant magnetization $\mathbf{m}(x,y) = m^o(\cos(\phi), \sin(\phi))$, $m^o = 0.02\,\mathrm{eV}$, and periodic boundary conditions. A Gaussian wave packet ($c\hbar k_x = 0.02\,\mathrm{eV}, k_y = 0$) is placed at the center of the simulation region, and its time evolution is monitored as a function of time. We have investigated the particle, spin, and current density. Note that the current density is perpendicular to the spin density. Here we will just show results for the particle density and plot functional (18) together with the norm of $\boldsymbol{\psi}$. Figure 4 shows the evolution of the wave packet as it propagates towards and across the boundaries of the simulation region. The simulation was performed on the Peierls transformed spinor exposed to the free-particle Dirac Hamiltonian. This corresponds to an exact implementation of the scheme. Due to the time independence of the magnetization only a single calculation of the phase factor is required, making this method very efficient. From Eq. (4) it is evident that in-plane magnetization can be absorbed into the vector potential contribution of the kinetic momentum [Eq. (2)] accounting for the change in propagation direction from horizontal to diagonal. The associated stability properties are shown in Fig. 5(a) where the conserved functional Eq. (18) and the lattice norm (trace) are plotted. Numerical values are normalized to the initial value. While the norm deviates slightly from its initial value conservation of the expression (18) is verified for the formal scheme. In contrast, the slowly varying-magnetic-field scheme diverges beyond time step 200, at a time when the wave packet has left the simulation region for the first time. The use of absorbing boundary conditions and/or a shorter time step will

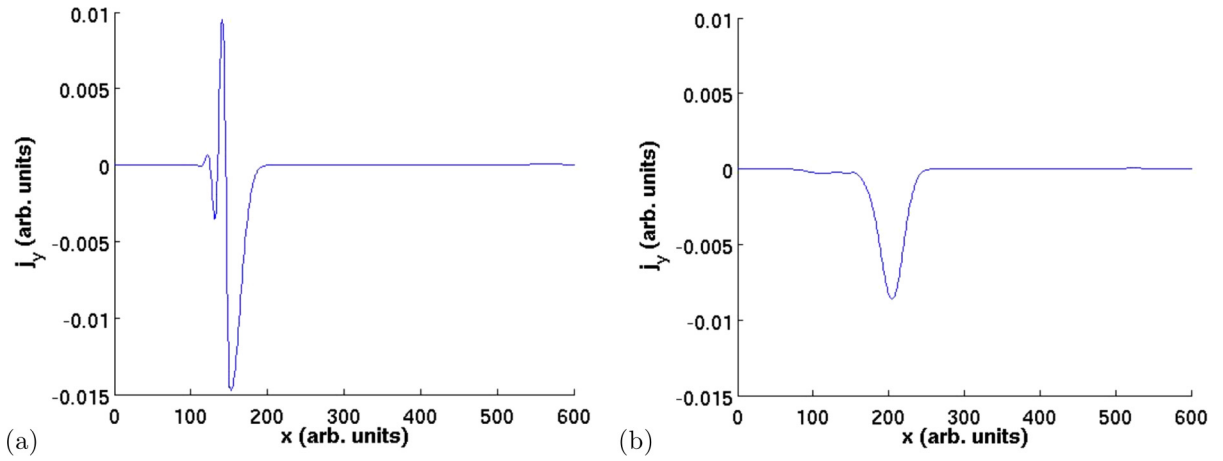

FIG. 6. Dirac fermion scattering at a magnetization step $m_x = -0.02\,\mathrm{eV}$, $m_y = m_z = 0$ under normal incidence, current density y component $j_y(x)$ versus x: (a) shortly after impinging on the magnetic domain boundary; (b) inside the magnetic domain [center of Fig. 5(a)].

suffice to suppress divergence for the duration of the physically relevant simulation (until the wave packet leaves the simulation region).

Finally, we simulate scattering of a Gaussian wave packet at a magnetization step $\mathbf{m}(x,y) = m^o\Theta(x - x_o)(\cos(\phi), \sin(\phi))$, $m^o = 0.02\,\mathrm{eV}$, $x_o \approx 200\,\mathrm{nm}$. The mean energy of the wave packet is $0.02\,\mathrm{eV}$. We set $\phi = \pi$. 600×600 grid points are chosen for a u-v time sheet pair. Again, the maximum permissible time step for stable evolution under the formal scheme is used. For this texture, the phase factor is path dependent and the static scheme is used for an implementation of Definition 2 on the grid. A comparison is made to the slowly varying-magnetic-field scheme. Figure 5 gives snap shots of the scattering process under the formal (static) scheme, as well as the data for trace and functional (30) from the static and slowly varying-magnetic-field scheme. Early time evolution is captured in good agreement between both methods, however, beyond time step 350 the slowly varying-magnetic-field simulation becomes unstable, while the static scheme preserves stability, as predicted theoretically.

Making closer contact with physical effects, we show the current density versus time in Fig. 6 from this simulation. Specifically, we display its y-component (transverse component) versus x shortly before the wave packet has entered the magnetization domain in Fig. 6(a). Figure 6(b) gives the transverse (y)-component of the current density versus x, shortly after the wave packet has impinged upon the magnetization step. Here one observes an effect typical for the Dirac equation [35,36]: In case of two counter-propagating wave contributions along x, there is an interference term which leads to a transverse current contribution along y, oscillating in position x. This is related to the Rashba effect associated with the spin-orbit interaction in the nonrelativistic limit [37].

VI. SUMMARY AND OUTLOOK

In summary, we have developed a single-cone finite-difference scheme for the (2+1)-dimensional time-dependent Dirac equation in the presence of general electromagnetic texture. The formal scheme is based on a Peierls-Schwinger substitution on a single-cone skeleton scheme. Under periodic or zero boundary conditions it allows a rigorous stability analysis based on an exactly conserved functional. In its original form it is applicable to static in-plane $(x - y)$ magnetic texture and general time-dependent scalar potential and mass terms. For time-dependent in-plane magnetic texture, three approximate schemes have been developed and compared with one another for selected basic numerical examples. Approximations are associated with the path dependence of line integrals in the Peierls-Schwinger phase factors. All of them share the properties of the skeleton scheme [1]: They are direct schemes, support a single (bounded) Dirac cone, and scale linearly in the number of grid points N. Among them, the double-update scheme is the most accurate regarding time resolution and stability.

This work lays the foundation for the time-dependent simulation of pure-state single-particle dynamics of Dirac fermions on TI surfaces. This method is readily extended to (3+1) dimensions, for application to problems in relativistic quantum mechanics, as well as to mixed-state transport simulations, and higher-order accurate schemes [30,38].

APPENDIX: DIFFERENCE SCHEME FOR THE (2+1)-DIMENSIONAL DIRAC EQUATION

Let ψ denote spinor component u or v, and the subscript $j = 1,2$ specify the grid point. Then one has the following relations for operations on the grid [1,27]:

(1) The effect of a substitution in difference quotients (derivative terms),

$$\frac{\psi_1 - \psi_2}{\Delta} \to \frac{e^{-ia_1}\psi_1 - e^{-ia_2}\psi_2}{\Delta},$$

can be expressed via the product rule for "differentiation on the lattice"

$$\frac{e^{-ia_1}\psi_1 - e^{-ia_2}\psi_2}{\Delta} = f_+(a_1,a_2)\frac{\psi_1 - \psi_2}{\Delta} + \frac{e^{-ia_1} - e^{-ia_2}}{\Delta}\frac{\psi_1 + \psi_2}{2},$$

with the definition $f_\pm(a_1,a_2) := (e^{-ia_1} \pm e^{-ia_2})/2$. For the case of slow variation of the phase a_j on the grid, the difference quotient for the exponential may be approximated by a "chain rule" for the derivative on the grid

$$\frac{e^{-ia_1} - e^{-ia_2}}{\Delta} = f_+(a_1,a_2)\frac{i(a_2-a_1)}{\Delta} + \frac{1}{\Delta}O[(a_1-a_2)^3]. \tag{A1}$$

(2) Symmetric averages of the form

$$\frac{\psi_1+\psi_2}{2} \to \frac{e^{-ia_1}\psi_1 + e^{-ia_2}\psi_2}{2}$$

may be recast into

$$\frac{e^{-ia_1}\psi_1 + e^{-ia_2}\psi_2}{2} = f_+(a_1,a_2)\frac{\psi_1+\psi_2}{2} + f_-(a_1,a_2)\frac{\psi_1-\psi_2}{2} \approx f_+(a_1,a_2)\frac{\psi_1+\psi_2}{2}. \tag{A2}$$

The f_- term may be neglected for sufficiently smooth phase a_i.

With the vector potential (and in-plane magnetization terms) introduced by the Peierls substitution, the scheme of Definition 2 expressed in terms of the original spinor components u and v is

$$\begin{aligned}
&f_+\big(a^{j_o+\frac{1}{2}}_{j_x,j_y}, a^{j_o-\frac{1}{2}}_{j_x,j_y}\big)\frac{\big(u^{j_o+\frac{1}{2}}_{j_x,j_y} - u^{j_o-\frac{1}{2}}_{j_x,j_y}\big)}{\Delta_o} \\
&= f_-\big(a^{j_o+\frac{1}{2}}_{j_x,j_y}, a^{j_o-\frac{1}{2}}_{j_x,j_y}\big)\left(\frac{m_z+V}{i\hbar c}\right)^{j_o}_{j_x,j_y}\frac{\big(u^{j_o+\frac{1}{2}}_{j_x,j_y} - u^{j_o-\frac{1}{2}}_{j_x,j_y}\big)}{2} \\
&\quad + \left[f_+\big(a^{j_o+\frac{1}{2}}_{j_x,j_y}, a^{j_o-\frac{1}{2}}_{j_x,j_y}\big)\left(\frac{m_z+V}{i\hbar c}\right)^{j_o}_{j_x,j_y} - \frac{2f_-\big(a^{j_o+\frac{1}{2}}_{j_x,j_y}, a^{j_o-\frac{1}{2}}_{j_x,j_y}\big)}{\Delta_o}\right]\frac{\big(u^{j_o+\frac{1}{2}}_{j_x,j_y} + u^{j_o-\frac{1}{2}}_{j_x,j_y}\big)}{2} \\
&\quad - f_+\big(a^{j_o}_{j_x,j_y+\frac{1}{2}}, a^{j_o}_{j_x,j_y-\frac{1}{2}}\big)\frac{\big(v^{j_o}_{j_x,j_y+\frac{1}{2}} - v^{j_o}_{j_x,j_y-\frac{1}{2}}\big)}{\Delta_y} - \frac{f_-\big(a^{j_o}_{j_x,j_y+\frac{1}{2}}, a^{j_o}_{j_x,j_y-\frac{1}{2}}\big)}{\Delta_y}\big(v^{j_o}_{j_x,j_y+\frac{1}{2}} + v^{j_o}_{j_x,j_y-\frac{1}{2}}\big) \\
&\quad - if_+\big(a^{j_o}_{j_x+\frac{1}{2},j_y}, a^{j_o}_{j_x-\frac{1}{2},j_y}\big)\frac{\big(v^{j_o}_{j_x+\frac{1}{2},j_y} - v^{j_o}_{j_x-\frac{1}{2},j_y}\big)}{\Delta_x} - i\frac{f_-\big(a^{j_o}_{j_x+\frac{1}{2},j_y}, a^{j_o}_{j_x-\frac{1}{2},j_y}\big)}{\Delta_x}\big(v^{j_o}_{j_x+\frac{1}{2},j_y} + v^{j_o}_{j_x-\frac{1}{2},j_y}\big),
\end{aligned} \tag{A3}$$

$$\begin{aligned}
&f_+\big(a^{j_o+\frac{1}{2}}_{j_x-\frac{1}{2},j_y-\frac{1}{2}}, a^{j_o-\frac{1}{2}}_{j_x-\frac{1}{2},j_y-\frac{1}{2}}\big)\frac{\big(u^{j_o+\frac{1}{2}}_{j_x-\frac{1}{2},j_y-\frac{1}{2}} - u^{j_o-\frac{1}{2}}_{j_x-\frac{1}{2},j_y-\frac{1}{2}}\big)}{\Delta_o} \\
&= f_-\big(a^{j_o+\frac{1}{2}}_{j_x-\frac{1}{2},j_y-\frac{1}{2}}, a^{j_o-\frac{1}{2}}_{j_x-\frac{1}{2},j_y-\frac{1}{2}}\big)\left(\frac{m_z+V}{i\hbar c}\right)^{j_o}_{j_x-\frac{1}{2},j_y-\frac{1}{2}}\frac{\big(u^{j_o+\frac{1}{2}}_{j_x-\frac{1}{2},j_y-\frac{1}{2}} - u^{j_o-\frac{1}{2}}_{j_x-\frac{1}{2},j_y-\frac{1}{2}}\big)}{2} \\
&\quad + \left[f_+\big(a^{j_o+\frac{1}{2}}_{j_x-\frac{1}{2},j_y-\frac{1}{2}}, a^{j_o-\frac{1}{2}}_{j_x-\frac{1}{2},j_y-\frac{1}{2}}\big)\left(\frac{m_z+V}{i\hbar c}\right)^{j_o}_{j_x-\frac{1}{2},j_y-\frac{1}{2}} - \frac{2f_-\big(a^{j_o+\frac{1}{2}}_{j_x-\frac{1}{2},j_y-\frac{1}{2}}, a^{j_o-\frac{1}{2}}_{j_x-\frac{1}{2},j_y-\frac{1}{2}}\big)}{\Delta_o}\right]\frac{\big(u^{j_o+\frac{1}{2}}_{j_x-\frac{1}{2},j_y-\frac{1}{2}} + u^{j_o-\frac{1}{2}}_{j_x-\frac{1}{2},j_y-\frac{1}{2}}\big)}{2} \\
&\quad - f_+\big(a^{j_o}_{j_x-\frac{1}{2},j_y}, a^{j_o}_{j_x-\frac{1}{2},j_y-1}\big)\frac{\big(v^{j_o}_{j_x-\frac{1}{2},j_y} - v^{j_o}_{j_x-\frac{1}{2},j_y-1}\big)}{\Delta_y} - \frac{f_-\big(a^{j_o}_{j_x-\frac{1}{2},j_y}, a^{j_o}_{j_x-\frac{1}{2},j_y-1}\big)}{\Delta_y}\big(v^{j_o}_{j_x-\frac{1}{2},j_y} + v^{j_o}_{j_x-\frac{1}{2},j_y-1}\big) \\
&\quad - if_+\big(a^{j_o}_{j_x,j_y-\frac{1}{2}}, a^{j_o}_{j_x-1,j_y-\frac{1}{2}}\big)\frac{\big(v^{j_o}_{j_x,j_y-\frac{1}{2}} - v^{j_o}_{j_x-1,j_y-\frac{1}{2}}\big)}{\Delta_x} - i\frac{\big(f_-(a^{j_o}_{j_x,j_y-\frac{1}{2}}, a^{j_o}_{j_x-1,j_y-\frac{1}{2}}\big)}{\Delta_x}\big(v^{j_o}_{j_x,j_y-\frac{1}{2}} + v^{j_o}_{j_x-1,j_y-\frac{1}{2}}\big),
\end{aligned} \tag{A4}$$

followed by

$$\begin{aligned}
&f_+\big(a^{j_o+1}_{j_x-\frac{1}{2},j_y}, a^{j_o}_{j_x-\frac{1}{2},j_y}\big)\frac{\big(v^{j_o+1}_{j_x-\frac{1}{2},j_y} - v^{j_o}_{j_x-\frac{1}{2},j_y}\big)}{\Delta_o} \\
&= f_-\big(a^{j_o+1}_{j_x-\frac{1}{2},j_y}, a^{j_o}_{j_x-\frac{1}{2},j_y}\big)\left(\frac{V-m_z}{i\hbar c}\right)^{j_o+\frac{1}{2}}_{j_x-\frac{1}{2},j_y}\frac{\big(v^{j_o+1}_{j_x-\frac{1}{2},j_y} - v^{j_o}_{j_x-\frac{1}{2},j_y}\big)}{2} \\
&\quad + \left[f_+\big(a^{j_o+1}_{j_x-\frac{1}{2},j_y}, a^{j_o}_{j_x-\frac{1}{2},j_y}\big)\left(\frac{V-m_z}{i\hbar c}\right)^{j_o+\frac{1}{2}}_{j_x-\frac{1}{2},j_y} - \frac{2f_-\big(a^{j_o+1}_{j_x-\frac{1}{2},j_y}, a^{j_o}_{j_x-\frac{1}{2},j_y}\big)}{\Delta_o}\right]\frac{\big(v^{j_o+1}_{j_x-\frac{1}{2},j_y} + v^{j_o}_{j_x-\frac{1}{2},j_y}\big)}{2}
\end{aligned}$$

$$
\begin{aligned}
&- f_+\left(a^{j_o+\frac{1}{2}}_{j_x-\frac{1}{2},j_y+\frac{1}{2}}, a^{j_o+\frac{1}{2}}_{j_x-\frac{1}{2},j_y-\frac{1}{2}}\right)\frac{\left(u^{j_o+\frac{1}{2}}_{j_x-\frac{1}{2},j_y+\frac{1}{2}} - u^{j_o+\frac{1}{2}}_{j_x-\frac{1}{2},j_y-\frac{1}{2}}\right)}{\Delta_y} - \frac{f_-\left(a^{j_o+\frac{1}{2}}_{j_x-\frac{1}{2},j_y+\frac{1}{2}}, a^{j_o+\frac{1}{2}}_{j_x-\frac{1}{2},j_y-\frac{1}{2}}\right)}{\Delta_y}\left(u^{j_o+\frac{1}{2}}_{j_x-\frac{1}{2},j_y+\frac{1}{2}} + u^{j_o+\frac{1}{2}}_{j_x-\frac{1}{2},j_y-\frac{1}{2}}\right)\\
&+ if_+\left(a^{j_o+\frac{1}{2}}_{j_x,j_y}, a^{j_o+\frac{1}{2}}_{j_x-1,j_y}\right)\frac{\left(u^{j_o+\frac{1}{2}}_{j_x,j_y} - u^{j_o+\frac{1}{2}}_{j_x-1,j_y}\right)}{\Delta_x} + i\frac{f_-\left(a^{j_o+\frac{1}{2}}_{j_x,j_y}, a^{j_o+\frac{1}{2}}_{j_x-1,j_y}\right)}{\Delta_x}\left(u^{j_o+\frac{1}{2}}_{j_x,j_y} + u^{j_o+\frac{1}{2}}_{j_x-1,j_y}\right),
\end{aligned}
\tag{A5}
$$

and

$$
\begin{aligned}
&f_+\left(a^{j_o+1}_{j_x,j_y-\frac{1}{2}}, a^{j_o}_{j_x,j_y-\frac{1}{2}}\right)\frac{\left(v^{j_o+1}_{j_x,j_y-\frac{1}{2}} - v^{j_o}_{j_x,j_y-\frac{1}{2}}\right)}{\Delta_o}\\
&= f_-\left(a^{j_o+1}_{j_x,j_y-\frac{1}{2}}, a^{j_o}_{j_x,j_y-\frac{1}{2}}\right)\left(\frac{V-m_z}{i\hbar c}\right)^{j_o+\frac{1}{2}}_{j_x,j_y-\frac{1}{2}}\frac{\left(v^{j_o+1}_{j_x,j_y-\frac{1}{2}} - v^{j_o}_{j_x,j_y-\frac{1}{2}}\right)}{2}\\
&\quad+\left[f_+\left(a^{j_o+1}_{j_x,j_y-\frac{1}{2}}, a^{j_o}_{j_x,j_y-\frac{1}{2}}\right)\left(\frac{V-m_z}{i\hbar c}\right)^{j_o+\frac{1}{2}}_{j_x,j_y-\frac{1}{2}} - \frac{2f_-\left(a^{j_o+1}_{j_x,j_y-\frac{1}{2}}, a^{j_o}_{j_x,j_y-\frac{1}{2}}\right)}{\Delta_o}\right]\frac{\left(v^{j_o+1}_{j_x,j_y-\frac{1}{2}} + v^{j_o}_{j_x,j_y-\frac{1}{2}}\right)}{2}\\
&\quad- f_+\left(a^{j_o+\frac{1}{2}}_{j_x,j_y}, a^{j_o+\frac{1}{2}}_{j_x,j_y-1}\right)\frac{\left(u^{j_o+\frac{1}{2}}_{j_x,j_y} - u^{j_o+\frac{1}{2}}_{j_x,j_y-1}\right)}{\Delta_y} - \frac{f_-\left(a^{j_o+\frac{1}{2}}_{j_x,j_y}, a^{j_o+\frac{1}{2}}_{j_x,j_y-1}\right)}{\Delta_y}\left(u^{j_o+\frac{1}{2}}_{j_x,j_y} + u^{j_o+\frac{1}{2}}_{j_x,j_y-1}\right)\\
&\quad+ if_+\left(a^{j_o+\frac{1}{2}}_{j_x+\frac{1}{2},j_y-\frac{1}{2}}, a^{j_o+\frac{1}{2}}_{j_x-\frac{1}{2},j_y-\frac{1}{2}}\right)\frac{\left(u^{j_o+\frac{1}{2}}_{j_x+\frac{1}{2},j_y-\frac{1}{2}} - u^{j_o+\frac{1}{2}}_{j_x-\frac{1}{2},j_y-\frac{1}{2}}\right)}{\Delta_x} + i\frac{f_-\left(a^{j_o+\frac{1}{2}}_{j_x+\frac{1}{2},j_y-\frac{1}{2}}, a^{j_o+\frac{1}{2}}_{j_x-\frac{1}{2},j_y-\frac{1}{2}}\right)}{\Delta_x}\left(u^{j_o+\frac{1}{2}}_{j_x+\frac{1}{2},j_y-\frac{1}{2}} + u^{j_o+\frac{1}{2}}_{j_x-\frac{1}{2},j_y-\frac{1}{2}}\right).
\end{aligned}
\tag{A6}
$$

[1] R. Hammer, W. Pötz, and A. Arnold, J. Comput. Phys. **265**, 50 (2014).
[2] R. Hammer, W. Pötz, and A. Arnold, J. Comput. Phys. **256**, 728 (2014).
[3] M. Creutz, Acta Physica Slovaca **61**, 1 (2011).
[4] J. Kogut and L. Susskind, Phys. Rev. D **11**, 395 (1975).
[5] P. H. Ginsparg and K. G. Wilson, Phys. Rev. D **25**, 2649 (1982).
[6] R. Stacey, Phys. Rev. D **26**, 468 (1982).
[7] D. B. Kaplan, Phys. Lett. B **288**, 342 (1992).
[8] J. W. Braun, Q. Su, and R. Grobe, Phys. Rev. A **59**, 604 (1999).
[9] G. R. Mocken and C. H. Keitel, Comput. Phys. Commun. **178**, 868 (2008).
[10] R. Beerwerth and H. Bauke, Comput. Phys. Commun. **188**, 189 (2015).
[11] A. C. Neto, F. Guinea, N. M. R. Peres, K. S. Novoselov, and A. K. Geim, Rev. Mod. Phys. **81**, 109 (2009), and references therein.
[12] M. Z. Hasan and C. L. Kane, Rev. Mod. Phys. **82**, 3045 (2010), and references therein.
[13] X. L. Qi and S. C. Zhang, Rev. Mod. Phys. **83**, 1057 (2011).
[14] D. Brinkman, C. Heitzinger, and P. A. Markowich, J. Comput. Phys. **257**, 318 (2014).
[15] Y. L. Chen *et al.*, Science **329**, 659 (2010).
[16] L. Barreto *et al.*, Nano Lett. **14**, 3755 (2014).
[17] A. Sulaev *et al.*, Nano Lett. **15**, 2061 (2015).
[18] K. Hoefer *et al.*, Proc. Natl. Acad. Sci. USA **111**, 14979 (2014).
[19] M. V. Costache, I. Neumann, J. F. Sierra, V. Marinova, M. M. Gospodinov, S. Roche, and S. O. Valenzuela, Phys. Rev. Lett. **112**, 086601 (2014).
[20] C.-Z. Chang *et al.*, Science **340**, 167 (2013).
[21] D. Culcer, Physica **E 44**, 860 (2012).
[22] C. H. Li, O. M. J. van't Erve, J. T. Robinson, Y. Liu, L. Li, and B. T. Jonker, Nat. Nanotechnol. **9**, 218 (2014).
[23] R. Hammer and W. Pötz, Phys. Rev. B **88**, 235119 (2013).
[24] H. J. Rothe, *Lattice Gauge Theories—An Introduction*, 3rd ed., World Scientific Lecture Notes in Physics (World Scientific, Singapore, 2005), Vol. 43.
[25] F. Fillion-Gourdeau, E. Lorin, and A. D. Bandrauk, Comput. Phys. Commun. **183**, 1403 (2012).
[26] H. B. Nielssen and M. Ninomiya, Phys. Lett. B **130**, 389 (1983).
[27] R. Hammer and W. Pötz, Comput. Phys. Commun. **185**, 40 (2014).
[28] O. Pinaud, J. Comput. Phys. **289**, 169 (2015).
[29] R. Peierls, Z. Phys. **80**, 763 (1933).
[30] W. Pötz and M. Schreilechner, J. Comput. Phys. **348**, 591 (2017).
[31] M. Graf and P. Vogl, Phys. Rev. B **51**, 4940 (1995), and references therein.
[32] J. D. Jackson, *Classical Electrodynamics*, 2nd ed. (Wiley, New York, 1975).
[33] B. DiBartolo, *Classical Theory of Electromagnetism* (Prentice-Hall, New Jersey, 1991).
[34] C. Cohen–Tannoudji, B. Diu, and F. Laloe, *Quantum Mechanics* (Hermann/Wiley, Paris, 1977).
[35] W. Greiner, *Relativistic Quantum Mechanics: Wave Equations* (Springer, Berlin, 2000).
[36] S. E. Savel'ev, W. Häusler, and P. Hänggi, Eur. Phys. J. B **86**, 433 (2013).
[37] G. Bihlmayer, O. Rader, and R. Winkler, New J. Phys. **17**, 050202 (2015).
[38] M. Schreilechner and W. Pötz, Comput. Phys. Commun. **204**, 43 (2016).